Hindawi
Structural Control and Health Monitoring
Volume 2024, Article ID 4930237, 23 pages
https://doi.org/10.1155/2024/4930237

Research Article

System Identification of a Structure Equipped with a Cable-Bracing Inerter System Using Adaptive Extended Kalman Filter

Rui Zhang,[1,2] **Songtao Xue**,[1,3] **Xinlei Ban**,[4] **Ruifu Zhang**,[1] **and Liyu Xie**[1]

[1]*Department of Disaster Mitigation for Structures, Tongji University, Shanghai 200092, China*
[2]*Department of Civil and Environmental Engineering, The Pennsylvania State University, University Park, PA 16802, USA*
[3]*Department of Architecture, Tohoku Institute of Technology, Sendai 982-8577, Japan*
[4]*Shanghai Electric Power Design Institute Co., Ltd., Shanghai 200025, China*

Correspondence should be addressed to Liyu Xie; liyuxie@tongji.edu.cn

Received 25 May 2023; Revised 17 January 2024; Accepted 19 January 2024; Published 9 February 2024

Academic Editor: Michael Krommer

An innovative cable-bracing inerter system (CBIS) has been proposed and shown to be effective in mitigating the structural response under dynamic excitation. The CBIS comprises an inerter element, an eddy current damping element, and a pair of tension-only cables that can transfer the story drift to rotating flywheels. To further investigate the characteristics of the CBIS, a system identification approach based on an adaptive extended Kalman filter (AEKF) and a recursive least-squares (RLS) algorithm is proposed. Depending on the CBIS model's availability, the proposed approach uses two strategies: the AEKF identifies the parameters of the structure and the CBIS when the model is specific; alternatively, when the model is unspecific, the KF combined with an RLS algorithm identifies the restoring force generated by the CBIS as an unknown fictitious input. In addition, the AEKF incorporates a time-variant fading factor to track the target adaptively. The proposed approach is validated through free vibration and shaking table tests, demonstrating the accuracy in identifying structural parameters and restoring force provided by the CBIS. The identification process involves two stages: initially, the AEKF identifies the parameters of the bare structure without the CBIS, followed by a dual strategy using either AEKF or KF-RLS for identifying the parameters of the CBIS or its restoring force, respectively. The findings also verify the feasibility and validity of the mechanical model and operating principle of the CBIS, thereby contributing to the advancement and application of the CBIS in future studies.

1. Introduction

Vibration control systems have been extensively developed and implemented to enhance the dynamic behavior of structures exposed to natural hazards, such as earthquakes [1, 2]. The effectiveness of these systems in mitigating seismic damage has been rigorously examined through shaking table tests [3–5]. However, there is limited research on the actual performance and energy dissipation capacity of vibration control systems during real earthquakes. The Great Eastern Japan Earthquake in 2011 provided a unique opportunity to investigate the performance of seismic protection technologies during a catastrophic earthquake [6]. During the Great Eastern Japan Earthquake in 2011, all the oil dampers on the first floor of an eight-story steel building were destroyed due to abutment breakage [7], prompting in-depth investigations into innovative devices and the real-world performance of vibration control systems [8, 9].

In recent years, inerter-based vibration control systems have emerged as an effective means of augmenting damping and magnifying mass effects in civil structures [10]. The concept of inerter was initially proposed by Smith [11] and referred to a two-terminal inertial element that generates an inertial force proportional to the relative acceleration between two terminals. Various inerter-based control systems have been developed using distinct methods to transform translational movement into rotational movement, including tuned viscous mass dampers, tuned mass-damper-

inerter systems, and tuned inerter dampers employing ball screws, rack pinions, and hydraulics for movement conversion, respectively [12–14].

While conventional viscous dampers primarily rely on viscous fluids for damping, they come with challenges, such as the cost of altering the damping coefficient and potential oil leakage [15]. To address these issues, researchers have turned to alternative damping mechanisms. The eddy current effect has emerged as a promising alternative, drawing attention for its numerous advantages, such as the absence of mechanical contact friction, stability at high temperatures, and its simplistic design [16, 17]. This effect is produced either by the relative motion between a nonmagnetic conductive material and a magnetic field or by the changing intensity of a stationary magnetic field [17, 18]. Recognizing its potential, eddy current dampers and eddy current-based tuned mass dampers have been proposed for engineering structures, capitalizing on their benefits, such as adjustability and stability [19–22].

To further enhance the efficiency of inerter systems, bracing systems have been used to convert translational movement into rotational movement between the structure and the inerter system [23]. Specifically, the cable-bracing systems have gained attention due to their tension-only and adjustable properties [24–26]. More recently, an innovative cable-bracing inerter system (CBIS) has been introduced and demonstrated to be effective in mitigating structural response through theoretical and experimental research [27–29]. The CBIS uses tension-only cables to convey the story drift to rotating flywheels (conductor plates) that function as the inerter. Additionally, the CBIS features an eddy current damper that dissipates vibration energy in the form of heat, resulting in a restoring force comprising the inertia force and the eddy current damping force. Nevertheless, additional research is required to validate the mechanical model of the CBIS and clarify the restoring force generated by the CBIS.

Identifying restoring forces is essential for evaluating the actual performance and energy dissipation capacity of vibration control systems. Extensive research has been conducted in this area, with comprehensive literature reviews available [30, 31]. Restoring force identification can be transformed into parameter identification problems when the models of the vibration control systems are specified, leaving only the coefficients of the model terms unspecified. For instance, extended Kalman filter- (EKF-) based methods are often used to identify parameters of linear or nonlinear hysteretic structures [32–34]. Alternatively, the restoring force generated by the vibration control systems can be treated as unknown fictitious input, which can be identified using input estimation techniques. This allows for the estimation of the model-free restoring forces without making prior assumptions or approximations about the vibration control systems. Recently, some KF-based methods with unknown input have been proposed to simultaneously estimate the system state and unknown input [35–41]. Particularly, several EKF-based model-free approaches have been developed to identify the restoring forces rather than the parameters of structural control systems [42–45].

Adaptive strategies are crucial in addressing the sensitivity of KF-based techniques to filter parameters. These methods are essential when dealing with unknown covariance matrices for process and measurement noises, as improper values can lead to estimation inaccuracies or divergence [46]. Moreover, in complex civil structures where modeling errors are inevitable, these errors can significantly impact model updating and predictions. Adaptive KF methods, categorized into Bayesian, maximum likelihood, correlation, and covariance-matching approaches offer potential solutions to these challenges [47–53]. Covariance-matching is a particularly effective method with successful applications in signal processing [54]. In particular, a strong tracking KF method with a time-variant fading factor based on the orthogonality principle is proposed, optimizing the filter's performance in the face of evolving uncertainties and noise [55–58].

This paper introduces an approach that explicitly defines the mechanical model and characterizes the behavior of the innovative CBIS. The approach incorporates an adaptive extended Kalman filter (AEKF) with a time-variant fading factor for estimating the structural state and the unknown structural parameters. Moreover, the KF can be combined with a recursive least-squares (RLS) algorithm for estimating the restoring force generated by the CBIS. To validate the performance of the proposed approach, free vibration tests and shaking table tests for a single degree-of-freedom (SDOF) structure equipped with a CBIS are conducted. The identification process initially uses the AEKF to identify the parameters of the bare structure without the CBIS. Following this, it engages both the AEKF and KF-RLS algorithms to determine the parameters of the CBIS or its restoring force, respectively.

2. Single Degree-of-Freedom Structure Equipped with a CBIS

2.1. Analysis Model of the CBIS. Figure 1 shows an SDOF structure with a CBIS, which includes a pair of tension-only cables, a pair of conductor plates (serve as flywheels), and a shaft. The tension-only cables connect the shaft and the structural frame diagonally, and when there is interstory drift, one of the cables will shorten and drive the shaft into rotation. The conductor plates are fixed on the shaft and rotate together with the shaft, acting as an inerter. Thus, the translational movement of the structure can be converted into a rotational motion of the inerter by cable bracing.

Meanwhile, as shown in Figure 1(b), serval magnets with alternating magnetic polarization are absorbed on the fixed side plates. Eddy currents, or Foucault currents, are generated when a conductor is exposed to a varying magnetic field, often due to its relative motion between the conductor and the magnetic source. These currents produce opposing magnetic fields, resulting in a repulsive force which is proportional to the relative velocity of the field and conductor, providing a damping effect [16–18]. In dynamic systems, the continuous motion of the conductor within the magnetic field leads to a consistent change in magnetic flux.

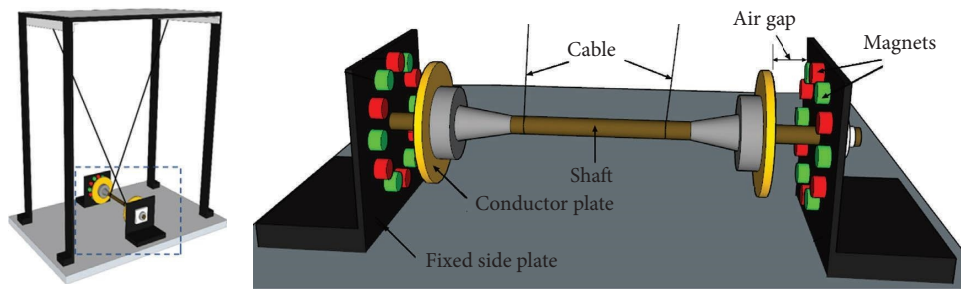

Figure 1: (a) An SDOF structure equipped with a CBIS and (b) details of the CBIS.

This induces currents that regenerate and dissipate as heat, allowing the system to function similarly to a viscous damper, removing energy from the system [19–22]. The eddy current damping force varies by adjusting the air gap between the magnets and the conducting plate.

Therefore, the CBIS can obtain its inertance and enhance the energy dissipation capacity via the eddy current damping. The effect of friction is ignored for simplicity; therefore, there are mainly three mechanical elements of the CBIS: an eddy current damping element, an inerter element, and a supporting spring element (cables). The damping element and the inerter element are connected in parallel and then connected in series with the spring element, as shown in Figure 2.

Therefore, the restoring force generated by the CBIS includes two main parts and can be calculated using the following equation:

$$F_d = k_b x_b = m_d \ddot{x}_d + c_d \dot{x}_d, \tag{1}$$

where F_d donates the restoring force generated by the CBIS and k_b and x_b donate the stiffness and the deformation of the spring element (cables), respectively. The first part is the inertial force, $m_d \ddot{x}_d$, where $\ddot{x}_d$ donates the relative acceleration response of the two terminals in the CBIS. The second part is the eddy current damping force, $c_d \dot{x}_d$, where c_d donates the equivalent damping coefficient of the CBIS, and $\dot{x}_d$ donates the relative velocity response of the two terminals in the CBIS.

2.2. Equation of Motion for an SDOF Structure Equipped with a CBIS. Figure 3(a) shows the layout and mechanical model of an SDOF structure equipped with a CBIS when the structure is deformed in a horizontal direction. In Figure 3(a), m, c, and k denote the mass, damping coefficient, and stiffness of the primary structure without a CBIS, respectively.

When the structure is in a balanced state, the prestressed tension forces in both cables are assumed as T_0. As shown in Figure 3(b), if the structure moves to the right with a relative horizontal displacement, the diagonal cable on the right side drives the shaft and conductor plate rotate clockwise. θ is the inclined angle of the diagonal cable. When the rotational angle of the conductor plate is φ, the axial elongation of the

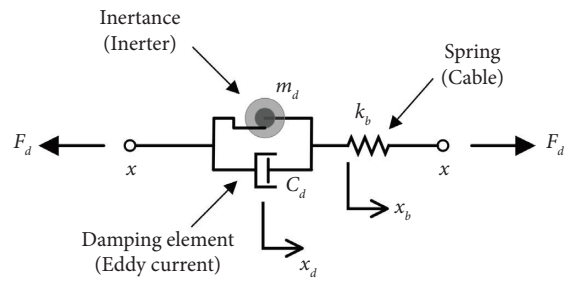

Figure 2: Mechanical model of the CBIS.

right cable is expressed as $x_b = x \cos\theta - \varphi r_0$. Considering the axial stiffness of each cable k_{b0}, the tension force in the right cable is increased as $T_2 = T_0 + k_{b0} x_b$, and the tension force in the left cable is decreased as $T_1 = T_0 - k_{b0} x_b$. Therefore, the restoring force generated by the CBIS is the tension force difference between two cables and can be expressed as $F_d = T_2 - T_1 = 2k_{b0} x_b = k_b x_b$, where k_b donates the equivalent stiffness of two cables.

According to the force equilibrium conditions and the layout of the system, the equation of motion for the SDOF structure with a CBIS can be represented as follows:

$$m\ddot{x} + c\dot{x} + kx + F_d \cos\theta = f, \tag{2}$$

where m, c, and k denote the mass, damping coefficient, and stiffness of the primary structure without a CBIS, respectively. Moreover, $\ddot{x}$, $\dot{x}$, and x denote the acceleration, velocity, and displacement of the SDOF system, respectively. $F_d \cos\theta$ is the restoring force in the horizontal direction generated by a CBIS, and f is the excitation force in the horizontal direction.

The motion equation for the CBIS, according to the rotational equilibrium condition of the CBIS, is expressed as follows:

$$J_d \ddot{\varphi} + c_I \dot{\varphi} r_0^2 = F_d r_0, \tag{3}$$

where J_d is the polar moment of inertia of the inerter, which can be calculated as $J_d = m_I R^2/2$. m_I is the physical mass of two conductor plates and the roller, and R is the radius of gyration. c_I is the damping coefficient of the CBIS, when the steel cables have a substantial stiffness, the analytical model of the CBIS can be simplified. The deformation of the cable is

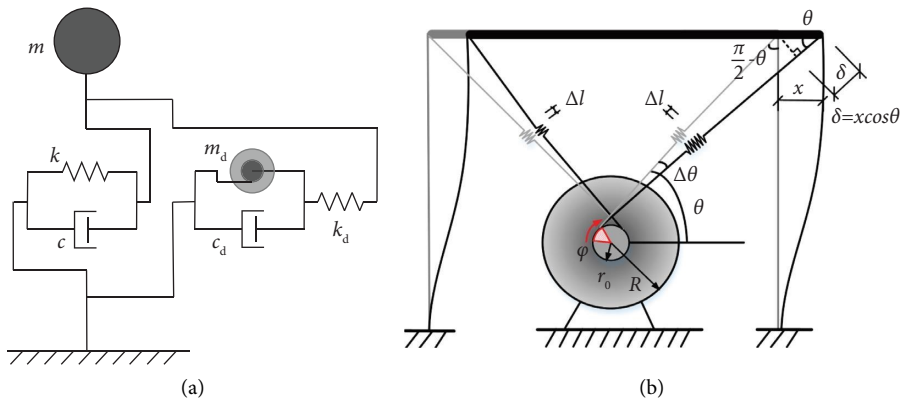

Figure 3: (a) Layout of an SDOF system equipped with a CBIS and (b) transmission mechanism of the CBIS.

neglected, and the relationship between the axial deformation of the cable and the rotational angle of the roller is given as follows:

$$\varphi = \frac{x\cos\theta}{r_0}. \tag{4}$$

Substituting equation (4) into equation (3), the restoring force generated by the CBIS, F_d, can be rewritten as follows:

$$\begin{aligned} F_d &= \frac{J_d\ddot{\varphi}}{r_0} + c_I\dot{\varphi}r_0 \\ &= \frac{J_d\cos\theta}{r_0^2}\ddot{x} + c_I\cos\theta\dot{x}. \end{aligned} \tag{5}$$

Therefore, the equation of motion of the SDOF structure equipped with a CBIS can be expressed as follows:

$$\begin{cases} m\ddot{x} + c\dot{x} + kx + f_d = f, \\ f_d = F_d\cos\theta = m_d\ddot{x} + c_d\dot{x}, \end{cases} \tag{6}$$

where m_d is the inertance of the CBIS, $m_d = J_d\cos^2\theta/r_0^2$, c_d is the equivalent damping coefficient in the horizontal direction of the CBIS, and $c_d = c_I\cos^2\theta$.

3. System Identification Based on Adaptive Kalman Filter

The general equation of motion of a multiple degrees-of-freedom (MDOF) structure equipped with the CBIS under external excitation can be expressed as follows:

$$\mathbf{M}\ddot{\mathbf{x}}(t) + \mathbf{C}\dot{\mathbf{x}}(t) + \mathbf{K}\mathbf{x}(t) + \mathrm{I}_d\mathbf{f}_d(t) = \mathrm{I}\mathbf{f}(t), \tag{7}$$

where $\mathbf{M}$ denotes the mass matrix of the structure and is assumed to be known, and $\mathbf{C}$ and $\mathbf{K}$ donate the damping matrix and stiffness matrix of the structure, respectively. $\ddot{\mathbf{x}}$, $\dot{\mathbf{x}}$, and $\mathbf{x}$ denote the acceleration, velocity, and displacement responses of the structure, respectively. $\mathbf{f}_d$ is the vector of the restoring force generated by the CBIS in the horizontal direction with an influence matrix $\mathbf{I}_d$. $\mathbf{f}$ is the vector of the external excitation with an influence matrix $\mathbf{I}$, which is assumed to be available in this study. The proposed technique contains two different strategies for two cases depending on the availability of the model of the CBIS.

3.1. Case 1: The Model of the CBIS Is Specific. When the model of the CBIS is specific, the restoring force generated by the CBIS in the horizontal direction can be expressed as $\mathbf{f}_d = \mathbf{M}_d\ddot{\mathbf{x}} + \mathbf{C}_d\dot{\mathbf{x}}$, where $\mathbf{M}_d$ and $\mathbf{C}_d$ denote the inertance and damping matrices of the CBIS, respectively. Therefore, the motion equation of an MDOF structure equipped with the CBIS, equation (7), can be rewritten as follows:

$$\mathbf{M}\ddot{\mathbf{x}}(t) + \mathbf{C}\dot{\mathbf{x}}(t) + \mathbf{K}\mathbf{x}(t) + \mathbf{I}_d\mathbf{M}_d\ddot{\mathbf{x}}(t) + \mathbf{I}_d\mathbf{C}_d\dot{\mathbf{x}}(t) = \mathbf{I}\mathbf{f}(t). \tag{8}$$

3.1.1. Structure State and Measurement Equations. The structural extended state vector is expressed as $\mathbf{Z} = \left\{\mathbf{x}^{\mathrm{T}}, \dot{\mathbf{x}}^{\mathrm{T}}, \boldsymbol{\theta}^{\mathrm{T}}\right\}^{\mathrm{T}}$, where $\boldsymbol{\theta}$ is the unknown structural parameters to be identified, including the stiffness and damping coefficient of the structure and the equivalent damping coefficient of the CBIS. Then, equation (8) can be transformed into a nonlinear state space as follows:

$$\begin{aligned} \dot{\mathbf{Z}} &= \begin{Bmatrix} \dot{\mathbf{x}}, \\ \ddot{\mathbf{x}}, \\ \dot{\theta}. \end{Bmatrix} \\ &= \begin{Bmatrix} \dot{\mathbf{x}} \\ (\mathbf{M} + \mathbf{I}_d\mathbf{M}_d)^{-1}\left[\mathbf{I}\mathbf{f} - (\mathbf{C} + \mathbf{I}_d\mathbf{C}_d)\dot{\mathbf{x}} - \mathbf{K}\mathbf{x}\right] \\ \mathbf{0} \end{Bmatrix} \\ &= g(\mathbf{Z}, \mathbf{f}) + \mathbf{w}, \end{aligned} \tag{9}$$

in which $\mathbf{w}$ is added to present the process noise with zero mean and a covariance matrix $\mathbf{Q} = E[\mathbf{w}\mathbf{w}^{\mathrm{T}}]$.

The measurement equation can be expressed as follows:

$$\mathbf{Y} = h(\mathbf{Z}, \mathbf{f}) + \mathbf{v}, \tag{10}$$

in which $\mathbf{Y}$ is an observation vector and $\mathbf{v}$ is the measurement noise with zero mean and a covariance matrix $\mathbf{R} = E[\mathbf{v}\mathbf{v}^{\mathrm{T}}]$. The state and measurement equations can be discretized over time intervals of length Δt, then equations

(9) and (10) can be linearized by Taylor series expansion to the first order at $\mathbf{Z}_{k-1} = \widehat{\mathbf{Z}}_{k-1}^{+}$ and $\mathbf{Z}_k = \widehat{\mathbf{Z}}_k^{-}$ as follows:

$$\begin{aligned} g(\mathbf{Z}_{k-1}, \mathbf{f}_{k-1}) &\approx g\left(\widehat{\mathbf{Z}}_{k-1}^{+}, \mathbf{f}_{k-1}\right) + \mathbf{G}_{k-1}\left(\mathbf{Z}_{k-1} - \widehat{\mathbf{Z}}_{k-1}^{+}\right), \\ h(\mathbf{Z}_k, \mathbf{f}_k) &\approx h\left(\widehat{\mathbf{Z}}_k^{-}, \mathbf{f}_k\right) + \mathbf{H}_k\left(\mathbf{Z}_k - \widehat{\mathbf{Z}}_k^{-}\right) + \mathbf{v}_k, \end{aligned} \tag{11}$$

in which $\widehat{\mathbf{Z}}_{k-1}^{+}$ and $\widehat{\mathbf{Z}}_k^{-}$ are the estimates of $\mathbf{Z}_{k-1}$ and $\mathbf{Z}_k$ at the time $t = (k-1)\Delta t$, respectively, and

$$\begin{aligned} \mathbf{G}_{k-1} &= \left.\frac{\partial \mathrm{g}(\mathbf{Z}, \mathbf{f})}{\partial \mathbf{Z}}\right|_{\mathbf{Z}=\widehat{\mathbf{Z}}_{k-1}^{+}}, \\ \mathbf{H}_k &= \left.\frac{\partial \mathrm{h}(\mathbf{Z}, \mathbf{f})}{\partial \mathbf{Z}}\right|_{\mathbf{Z}=\widehat{\mathbf{Z}}_k^{-}}. \end{aligned} \tag{12}$$

3.1.2. Adaptive Extended Kalman Filter. When the model of the CBIS is specific, the Kalman filter-based techniques can be employed for estimating the state and unknown parameters of both the structure and the CBIS. Kalman-type filters are effective when the prior knowledge, including reference models, noise distribution, and initial conditions, is accurate. If prior knowledge is not available or inaccurate, the Kalman-type filters may suffer performance degradation or instability, as the prior knowledge does not match the behavior of the controlled system. To overcome this challenge, an adaptive extended Kalman filter (AEKF) with a time-variant fading factor is introduced.

First, based on the model and the observations until time $\mathbf{t} = (k-1)\Delta t$, the prediction of the state at the time $\mathbf{t} = k\Delta t$ can be obtained.

$$\widehat{\mathbf{Z}}_k^{-} = \widehat{\mathbf{Z}}_{k-1}^{+} + \int_{(k-1)\Delta t}^{k\Delta t} g\left(\widehat{\mathbf{Z}}_{t|k-1}, \mathbf{f}\right)\mathrm{d}t, \tag{13}$$

$$\widehat{\mathbf{P}}_k^{-} = \lambda_k \boldsymbol{\Phi}_{k-1} \widehat{\mathbf{P}}_{k-1}^{+} \boldsymbol{\Phi}_{k-1}^{T} + \mathbf{Q}_{k-1}, \tag{14}$$

where $\widehat{\mathbf{P}}_{k-1}^{+}$ and $\widehat{\mathbf{P}}_k^{-}$ are the error covariance matrices of $\widehat{\mathbf{Z}}_{k-1}^{+}$ and $\widehat{\mathbf{Z}}_k^{-}$, respectively. The nonlinear term in equation (13) can be linearized by Taylor's expansion, which is resolved using the fourth-order Runge–Kutta method in this paper. $\boldsymbol{\Phi}_{k-1}$ is the state transition matrix of the linearized system, $\boldsymbol{\Phi}_{k-1} = \exp(\mathbf{G}_{k-1}\Delta t)$. As shown in equation (14), a fading factor λ_k is introduced to modify the error covariance matrix $\widehat{\mathbf{P}}_k^{-}$, and the determination of λ_k will be discussed in detail in the next section.

Then, using the new information provided by the observation at the time $t = k\Delta t$, the updated prediction at the time $t = k\Delta t$ can be obtained as follows:

$$\widehat{\mathbf{Z}}_k^{+} = \widehat{\mathbf{Z}}_k^{-} + \mathbf{K}_k\left[\mathbf{Y}_k - h\left(\widehat{\mathbf{Z}}_k^{-}, \mathbf{f}\right)\right], \tag{15}$$

$$\mathbf{K}_k = \widehat{\mathbf{P}}_k^{-}\mathbf{H}_k^{\mathrm{T}}\left(\mathbf{H}_k\widehat{\mathbf{P}}_k^{-}\mathbf{H}_k^{\mathrm{T}} + \mathbf{R}_k\right)^{-1}, \tag{16}$$

$$\widehat{\mathbf{P}}_k^{+} = \left(\mathbf{I} - \mathbf{K}_k\mathbf{H}_k\right)\widehat{\mathbf{P}}_k^{-}\left(\mathbf{I} - \mathbf{K}_k\mathbf{H}_k\right)^{\mathrm{T}} + \mathbf{K}_k\mathbf{R}_k\mathbf{K}_k^{\mathrm{T}}, \tag{17}$$

where $\mathbf{Y}_k$ is the measurement vector, $\widehat{\mathbf{Z}}_k^{+}$ is the estimate of $\mathbf{Z}_k$ at the time $t = k\Delta t$, $\mathbf{K}_k$ is the Kalman gain, and $\widehat{\mathbf{P}}_k^{+}$ is the error covariance matrix of $\widehat{\mathbf{Z}}_k^{+}$.

3.1.3. Determination of the Fading Factor. The determination of the fading factor is detailed in this subsection. As shown in equation (14), a fading factor λ_k is introduced to modify the error covariance matrix $\widehat{\mathbf{P}}_k^{-}$ to amplify the Kalman gain. However, the fading factor λ_k is sensitive to noise if the λ_k is small, or it will have less tracking capability if the λ_k is large. Various methodologies exist for constructing and solving adaptive factors or matrices. Mehra [47] categorized adaptive approaches into four distinct groups: Bayesian, maximum likelihood, correlation, and covariance matching. In both correlation and covariance-matching techniques, innovation sequences have played a vital role in estimating noise covariances. The fundamental concept underlying the covariance-matching approach revolves around ensuring that the actual covariance of the residual aligns with its theoretical value.

Particularly, a strong tracking filtering was proposed to enhance the filter's efficacy by real-time adjustments to the error covariance matrix and gain matrix using a time-variant fading factor or matrix [55–58]. To be specific, the time-variant fading factor λ_k is determined by solving the following optimization problem:

$$\begin{aligned} E\left[\mathbf{Z}_k - \widehat{\mathbf{Z}}_k\right]\left[\mathbf{Z}_k - \widehat{\mathbf{Z}}_k\right]^T &= \min, \\ E\left[\boldsymbol{\varepsilon}_{k+j}\boldsymbol{\varepsilon}_k^{\mathrm{T}}\right] &= 0, \end{aligned} \tag{18}$$

where $\boldsymbol{\varepsilon}_k$ is the innovation residual sequence, $\boldsymbol{\varepsilon}_k = \mathbf{Y}_k - \widehat{\mathbf{Y}}_k^{-}$, defined as the difference between considering incoming measurements $\mathbf{Y}_k$ and the optimal predictions $\widehat{\mathbf{Y}}_k^{-}$ obtained in the preceding step. The cost function in equation (18) is the optimal rule of the state estimation, and the constraint means that the innovation residual vector should be orthogonal to each other at each step. The physical meaning is that all the meaningful information can be extracted from the innovation residual sequence.

While obtaining an exact solution for the optimization problem described by equation (18) is challenging, a viable suboptimal solution can be expressed as follows:

$$\lambda_k = \begin{cases} \lambda_{0,k}, & \lambda_{0,k} \geq 1, \\ 1, & \lambda_{0,k} < 1, \end{cases} \tag{19}$$

where λ_k should be no less than 1, when it equals 1, the AEKF is the conventional EKF. $\lambda_{0,k}$ can be calculated using equation (20), with detailed derivations provided in Appendix A.

$$\lambda_{0,k} = \frac{\mathrm{tr}\left[\mathbf{V}_k - \mathbf{H}_k\mathbf{Q}_{k-1}\mathbf{H}_k^{\mathrm{T}} - \mathbf{R}_k\right]}{\mathrm{tr}\left[\mathbf{H}_k\boldsymbol{\Phi}_{k-1}\mathbf{P}_{k-1}^{+}\boldsymbol{\Phi}_{k-1}^{\mathrm{T}}\mathbf{H}_k^{\mathrm{T}}\right]}. \tag{20}$$

Furthermore, $\mathbf{V}_k$ is the covariance matrix of the estimated output error, $\mathbf{V}_k = E[\boldsymbol{\varepsilon}_k\boldsymbol{\varepsilon}_k^{\mathrm{T}}]$. $\mathbf{V}_k$ will increase as any

parameters vary. Therefore, in order to reflect the change of $\mathbf{V}_k$ and the importance of the current measured data, the weighting factor $\boldsymbol{\alpha}$ is used to calculate the $\mathbf{V}_k$ as follows:

$$\mathbf{V}_k = \begin{cases} \boldsymbol{\varepsilon}_1 \boldsymbol{\varepsilon}_1^{\mathrm{T}}, & k = 1, \\ \dfrac{\alpha \mathbf{V}_{k-1} + \boldsymbol{\varepsilon}_k \boldsymbol{\varepsilon}_k^{\mathrm{T}}}{1+\alpha}, & k \geq 2, \end{cases} \tag{21}$$

in which α is a weighting factor $(0 < \alpha \leq 1)$, indicating the importance of the measured data near $t = k\Delta t$, and it is commonly set as 0.95 [55–58].

3.2. Case 2: The Model of the CBIS Is Unspecific. When the model of the CBIS is assumed to be unknown, and the restoring force provided by the CBIS in the horizontal direction can be considered as "unknown fictitious input," $\mathbf{f}_d$, on the bare structure without the CBIS. The motion equation is shown in equation (7), and the mass, stiffness, and damping parameters of the linear bare structure are all assumed as known values. Kalman filter (KF) and recursive least-squares (RLS) algorithm, denoted as KF-RLS, was introduced to identify structural states and unknown restoring force provided by the CBIS.

3.2.1. Structure State and Measurement Equations. Define structural state vector by $\mathbf{Z}(t) = \left\{\mathbf{x}^{\mathrm{T}}, \dot{\mathbf{x}}^{\mathrm{T}}\right\}^{\mathrm{T}}$. From equation (8), the continuous-time state equations and measurement equations can be written as follows:

$$\begin{aligned} \dot{\overline{\mathbf{Z}}} &= \begin{bmatrix} \mathbf{0} & \mathbf{I} \\ -\mathbf{M}^{-1}\mathbf{K} & -\mathbf{M}^{-1}\mathbf{C} \end{bmatrix} \begin{Bmatrix} \mathbf{x} \\ \dot{\mathbf{x}} \end{Bmatrix} + \begin{Bmatrix} \mathbf{0} \\ \mathbf{M}^{-1}\mathrm{I} \end{Bmatrix} \mathbf{f} + \begin{Bmatrix} \mathbf{0} \\ -\mathbf{M}^{-1}\mathrm{I}_d \end{Bmatrix} \mathbf{f}_d \\ &= \mathbf{A}\overline{\mathbf{Z}} + \mathbf{B}\mathbf{f} + \mathbf{B}_d\mathbf{f}_d. \end{aligned} \tag{22}$$

The state equation can be further discretized over time intervals of length Δt and rewritten as follows:

$$\mathbf{Z}_k = \overline{\boldsymbol{\Phi}}\mathbf{Z}_{k-1} + \Gamma \mathbf{f}_{k-1} + \Gamma_d\left(\mathbf{f}_{d,k-1} + \overline{\mathbf{w}}_{k-1}\right), \tag{23}$$

in which $\overline{\boldsymbol{\Phi}}$ is the state transformation matrix, $\overline{\boldsymbol{\Phi}} = \exp(\mathbf{A}\Delta t)$, Γ and Γ_d are the influence matrices of $\mathbf{f}_{k-1}$ and $\mathbf{f}_{d,k-1}$, respectively, and expressed as follows:

$$\Gamma_d = \int_{k\Delta t}^{(k+1)\Delta t} \exp\{\mathbf{A}[(k+1)\Delta t - \tau]\}\mathbf{B}_d d\tau, \tag{24}$$

in which $\overline{\mathbf{w}}$ is added to present the process noise with zero mean and a covariance matrix $\overline{\mathbf{Q}} = E[\overline{\mathbf{w}}\overline{\mathbf{w}}^{\mathrm{T}}]$. The measurement equation can be expressed as follows:

$$\overline{\mathbf{Y}}_k = \overline{\mathbf{H}}_k\mathbf{Z}_k + \overline{\mathbf{v}}_k, \tag{25}$$

in which $\overline{\mathbf{H}}_k$ is the measurement matrix of $\overline{\mathbf{Z}}_{k+1}$ and $\overline{\mathbf{v}}$ is added to present the measurement noise with zero mean and a covariance matrix $\overline{\mathbf{R}} = E[\overline{\mathbf{v}}\overline{\mathbf{v}}^{\mathrm{T}}]$. It is important to note that the covariance matrices utilized in the AEKF and KF-RLS are different.

3.2.2. Kalman Filter with Recursive Least-Squares. To identify the unknown restoring force $\mathbf{f}_d$ generated by the CBIS, this paper proposed a KF-RLS algorithm. First, the KF is used to generate the innovation residual sequence. Following the general KF equations, the priori state estimations of $\mathbf{Z}_k$ without and with $\mathbf{f}_d$ are donated as $\overline{\mathbf{Z}}_k^-$ and $\widehat{\mathbf{Z}}_k^-$, respectively, and are expressed as follows:

$$\overline{\mathbf{Z}}_k^- = \overline{\boldsymbol{\Phi}}\overline{\mathbf{Z}}_{k-1}^+ + \Gamma \mathbf{f}_{k-1}, \tag{26}$$

$$\widehat{\mathbf{Z}}_k^- = \boldsymbol{\Phi}\widehat{\mathbf{Z}}_{k-1}^+ + \Gamma \mathbf{f}_{k-1} + \Gamma_d \mathbf{f}_{d,k-1}. \tag{27}$$

The error covariance matrix is expressed as follows:

$$\widehat{\mathbf{P}}_k^- = \overline{\boldsymbol{\Phi}}\widehat{\mathbf{P}}_{k-1}^+\overline{\boldsymbol{\Phi}}^{\mathrm{T}} + \Gamma_d\overline{\mathbf{Q}}\Gamma_d^{\mathrm{T}}. \tag{28}$$

Then, using the new information provided by the observation at the time $t = k\Delta t$, the updated prediction at the time $t = k\Delta t$ can be obtained as follows:

$$\overline{\mathbf{Z}}_k^+ = \overline{\mathbf{Z}}_k^- + \mathbf{K}_k\overline{\mathbf{Y}}_k = \overline{\mathbf{Z}}_k^- + \mathbf{K}_k\left(\mathbf{Y}_k - \mathbf{H}_k\overline{\mathbf{Z}}_k^-\right), \tag{29}$$

$$\widehat{\mathbf{Z}}_k^+ = \widehat{\mathbf{Z}}_k^- + \mathbf{K}_k\widehat{\mathbf{Y}}_k = \widehat{\mathbf{Z}}_k^- + \mathbf{K}_k\left(\mathbf{Y}_k - \mathbf{H}_k\widehat{\mathbf{Z}}_k^-\right), \tag{30}$$

where $\overline{\mathbf{Z}}_k^+$ and $\widehat{\mathbf{Z}}_k^+$ are the posterior estimations of $\mathbf{Z}_k$ without and with $\mathbf{f}_{d,k-1}$, respectively. $\mathbf{K}_k$ is the Kalman gain calculated by equation (16). $\overline{\mathbf{Y}}_k$ and $\widehat{\mathbf{Y}}_k$ are the innovation residual sequences without and with $\mathbf{f}_{d,k-1}$, respectively. The recursive relationshipn among $\overline{\mathbf{Y}}_k$, $\widehat{\mathbf{Y}}_k$, and the unknown $\mathbf{f}_d$ can be expressed by equation (31), with detailed derivations provided in Appendix B.

$$\overline{\mathbf{Y}}_k = \widehat{\mathbf{Y}}_k + \mathbf{B}_k\mathbf{f}_{d,k-1}, \tag{31}$$

where $\mathbf{B}_k$ and $\mathbf{M}_k$ are defined as the sensitivity matrices and expressed as follows:

$$\mathbf{B}_k = \mathbf{H}_k\left(\mathbf{A}\mathbf{M}_{k-1} + \mathbf{I}\right)\mathbf{B}_d, \tag{32}$$

$$\mathbf{M}_k = \left(\mathbf{I} - \mathbf{H}_k\mathbf{K}_k\right)\left(\mathbf{A}\mathbf{M}_{k-1} + \mathbf{I}\right). \tag{33}$$

Then, the RLS algorithm can be used to compute the onset time histories of the unknown restoring force with the equations as follows:

$$\mathbf{K}_k^* = \frac{\mathbf{P}_{k-1}^*\mathbf{B}_k^{\mathrm{T}}}{\rho}\left[\frac{\mathbf{B}_k\mathbf{P}_{k-1}^*\mathbf{B}_k^{\mathrm{T}}}{\rho} + \mathbf{S}_k\right]^{-1}, \tag{34}$$

$$\mathbf{P}_k^* = \frac{1}{\rho}\left[\mathbf{I} - \mathbf{K}_k^*\mathbf{B}_k\right]\mathbf{P}_{k-1}^*, \tag{35}$$

$$\widehat{\mathbf{f}}_{d,k} = \widehat{\mathbf{f}}_{d,k-1} + \mathbf{K}_k^*\left[\mathbf{Y}_k - h\left(\widehat{\mathbf{Z}}_k^-, \mathbf{f}\right) - \mathbf{B}_k\widehat{\mathbf{f}}_{d,k-1}\right], \tag{36}$$

where $\mathbf{K}_k^*$ and $\mathbf{P}_k^*$ are the correction Kalman gain and the error covariance of the estimated restoring force vector $\widehat{\mathbf{f}}_{d,k}$. A forgetting factor ρ, $0 < \rho \leq 1$, utilized in this algorithm, acts as a regulator to adjust the correction Kalman gain $\mathbf{K}_k^*$ or filter bandwidth for overcoming the destructive influence of process noise $\overline{\mathbf{R}}$, measurement noise $\overline{\mathbf{Q}}$, and input disturbance in the output of KF [59, 60]. Then, this updated

estimated value is fed into structural model to correct the system output of the KF algorithm and, subsequently, and optimal estimate $\widehat{\mathbf{f}}_{d,k}$ can be obtained.

When $\rho = 1$, the above algorithm reduces to that of the conventional sequential least-squares algorithm, which is appropriate only for a constant input estimation. In this case, the correction Kalman gain $\mathbf{K}_k^*$ for updating $\widehat{\mathbf{f}}_d$ in equation (34) decreases with an increasing k. For $0 < \rho < 1$, $\mathbf{K}_k^*$ has been effectively prevented from shrinking to zero. Hence, the corresponding algorithm can preserve its updating ability continuously and fit for time varying input estimation. However, the inherent data truncation effect due to ρ causes variance increases in $\widehat{\mathbf{f}}_d$ attributed to noise. Thus, a compromise must be made between rapid adaptive capability and the loss of estimation accuracy [61, 62].

3.3. Summary. In conclusion, the identification approach presented in this study integrates two techniques that are the AEKF and KF-RLS. For case 1, when the model of the CBIS is specific, the AEKF can be used for estimating the state and unknown parameters of both the structure and the CBIS. The AEKF consists of prediction and update stages, which can be summarized as follows: (1) the structure state and measurement equations is calculated using equations (9) and (10); (2) in the prediction stage, the AEKF uses the state estimate from the previous timestep to generate an estimate of the state at the current timestep, calculated using equations (13) and (14); (3) in the update stage, the residual difference between the current prediction and the current observation information is combined to refine the state estimate, calculated using equations (15)–(17); and (4) the adaptive fading factor is calculated using equations (19)–(21).

For case 2, when the model of the vibration control system is unspecific, the KF-RLS can be used for estimating the state and unknown restoring force generated by the CBIS. The KF-RLS consists of two stages, which can be summarized as follows: (1) the structure state and measurement equations are calculated using equations (22)–(24); (2) the KF can first be utilized to obtain a recursive relationship between the innovation residual sequences and the unknown restoring $\mathbf{f}_d$, using equations (31)–(33); (3) finally, the RLS algorithm with the forgetting factor is applied to calculate the unknown force $\widehat{\mathbf{f}}_d$ using equations (34)–(36).

In this study, either structural acceleration or displacement can be chosen as observations. Using only the structural acceleration responses as observations can sometimes result in low-frequency drift in the identification results [36, 63]. However, these results can be significantly enhanced when the observations incorporate partial structural displacement or strain measurements [41, 64, 65]. For Case 1, we use AEKF and use only acceleration responses as observations. For case 2, we utilize KF-RLS and rely solely on displacement responses. Nonetheless, for optimal identification results, especially in the presence of noisy observations, it is recommended to include both structural acceleration and displacement (or strain) in the observation vector.

4. Numerical Simulation

To illustrate the effectiveness and accuracy of the proposed approach in estimating unknown structural parameters and restoring forces generated by CBIS, numerical experiments of a four-degree-of-freedom dynamic system are analyzed (Figure 4).

The equation of motion of the MDOF structure equipped with CBIS is expressed in equation (7). The system is subjected to the El Centro earthquake ground excitation with a peak ground acceleration of 0.2 g (g is the acceleration due to gravity). The mass, story stiffness, and damping coefficients of each story are assumed to be $m_i = 300\,\text{kg}$, $k_i = 15000\,\text{N/m}$, $\mathbf{C} = \alpha\mathbf{M} + \beta\mathbf{K}$ with $\alpha = 0.3$, and $\beta = 0.0025$, respectively. The building is equipped with the CBIS for each story. The equivalent damping coefficient and inertance of the CBIS for each story is $c_{di} = 20\,\text{N/m/s}$ and $m_{di} = 100\,\text{kg}$, respectively. Two case studies are presented depending on the availability of the model of the CBIS, which correspond with the two different approaches, respectively.

4.1. Case 1: The Model of the CBIS Is Specific. In the first case, it is assumed that the model of the CBIS and the inertance of the CBIS, m_{di}, for each story are known. Additionally, the mass of each story, m_i, is also assumed to be known. The inputs for the identification problem are the acceleration responses for all the floors. The goal is to estimate the full states of the structure and the unknown parameters of the structure and CBIS, including k_i, c_{di}, α, and β, using the AEKF. The extended state vector is expressed as $\mathbf{Z} = [x_1, \cdots, x_4, \dot{x}_1, \cdots, \dot{x}_4, c_{d1}, \cdots, c_{d4}, k_1, \cdots, k_4, \alpha, \beta]^{\mathrm{T}}$. The parameters used in the AEKF are given as follows: zero initial conditions, sampling interval $\Delta t = 0.02\,s$, and the initial error covariance matrix $\mathbf{P} = 10^3\mathbf{I}_{18\times18}$. The initial values of the unknown parameters were all chosen to be 50% of the corresponding actual ones. Once the parameters of the CBIS are identified using the AEKF, the restoring forces by the CBIS can then be calculated using the equation of $\mathbf{f}_d = \mathbf{M}_d\ddot{\mathbf{x}} + \mathbf{C}_d\dot{\mathbf{x}}$.

The accurate determination of the covariance matrices $\mathbf{R}$ and $\mathbf{Q}$ is critical for the performance and convergence of the Kalman filter estimation process [47, 66, 67]. These matrices are typically estimated by analyzing the statistical properties of the measurement and process noise, informed by extensive experimentations [68]. For instance, the authors in references [36, 69] suggested that these matrices should be determined based on the accuracy of the sensors and the order of magnitude of the state vector, respectively.

The $\mathbf{R}$ matrix reflects the confidence in sensor measurements, with a smaller $\mathbf{R}$ value indicating greater trust in the observed data [69]. In this study, the noisy measured responses, donated as $\mathbf{Y}$, are simulated using the Newmark beta method and contaminated with zero-mean Gaussian white noise at a 5% root-mean-square (RMS) level, which informs the calibration of the $\mathbf{R}$ matrix to $\mathbf{R} = (5\% \times \text{RMS}(\mathbf{Y}))^2$ [67–70]. Consequently, with an RMS value of measured accelerations being $\mathbf{RMS}(\mathbf{Y}) \approx 0.64$, $\mathbf{R}$ is calculated as $\mathbf{R} = 10^{-3}\mathbf{I}_{4\times4}$.

Conversely, the $\mathbf{Q}$ matrix reveals the confidence in the system model, and a smaller $\mathbf{Q}$ value implies a more accurate model. Discretization errors, which are a significant source

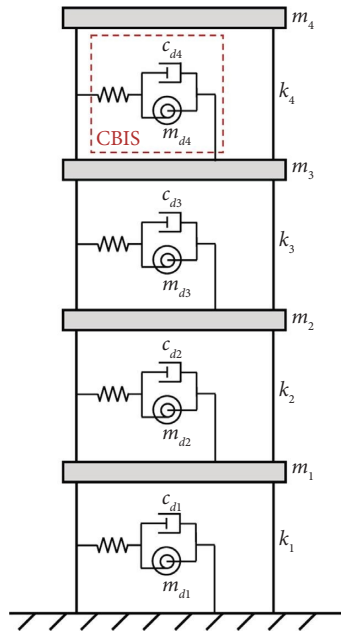

Figure 4: Analysis model of an MDOF structure with CBIS.

of process noise, diminish with smaller timestep intervals, allowing $\mathbf{Q}$ to be set to a minimal value [51, 70]. Even though for systems with static parameters, the process noise covariance could theoretically be zero, a slight but nonzero $\mathbf{Q}$ value is recommended to enhance the speed of parameter convergence [71]. Therefore, in the simulations where the model deployed in the algorithms is assumed to be accurate, the process noise is set to a small value of $\mathbf{Q} = 10^{-8}\mathbf{I}_{18\times18}$. It has been observed through case studies that a $\mathbf{Q}$ value lesser than $\mathbf{Q} = 10^{-5}\mathbf{I}_{18\times18}$ did not significantly degrade the quality of estimation, thus attesting to the robustness of the method.

Table 1 presents the comparison of the identified parameters k_i, α, and β for the structure, along with c_{di} for the CBIS for each story, using both AEKF and EKF approaches. The comparison results illustrate that the conventional EKF, with $\mathbf{Q} = 10^{-8}\mathbf{I}_{18\times18}$, can identify the k_i and α with high accuracy. However, it fails to estimate the exact values of β and c_{di}. Figure 5 illustrates the calculated adaptive fading factor used in the AEKF, varying between 1 and 1.4 over time. As shown in Table 1, the proposed AEKF with the adaptive fading factor can identify all the parameters in a high accuracy when the $\mathbf{Q}$ value is lesser than $\mathbf{Q} = 10^{-5}\mathbf{I}_{18\times18}$.

Figures 6(a)–6(f) show the convergence processes of the parameters using AEKF and EKF, with a focus on the second and fourth floors due to the limitation of paper length. The estimated responses and restoring forces are presented in Figures 7(a)–7(f). The comparison of the estimations and the ground truth suggests that the tracking capability of the proposed technique is plausible.

4.2. Case 2: The Model of the CBIS Is Unspecific. In the second case, the model of the damper is assumed to be unknown, and the restoring force provided by the damper is treated as unknown fictitious input. The inputs for the restoring force identification problem are deflection responses for all the floors in this case. The goal is to estimate the full states of the structure and the unknown restoring force provide by the CBIS, $\mathbf{f}_d$, using the KF-RLS. The parameters used in the KF-RLS are given as follows: zero initial conditions, sampling interval $\Delta t = 0.02$ s, and the initial values of the matrices are $\mathbf{P}_{k,0} = 10^{10}\mathbf{I}_{8\times8}$, $\mathbf{P}^*_{k,0} = 10^{10}\mathbf{I}_{4\times4}$, and $\mathbf{M}_{k,0} = \mathbf{0}_{8\times8}$, respectively.

In these simulations, the deflection responses were calculated using the Newmark beta method and were contaminated with zero-mean Gaussian white noise at a 5% RMS level. Consequently, the $\overline{\mathbf{R}}$ matrix is calculated as $\overline{\mathbf{R}} = (5\% \times \mathrm{RMS}(\mathbf{Y}))^2 \approx 10^{-8}\mathbf{I}_{4\times4}$. It is essential to distinguish between the $\overline{\mathbf{Q}}$ matrix used in the KF-RLS and the $\mathbf{Q}$ matrix in the AEKF. As specified in equations (23) and (28), the equivalent covariance matrix is formulated as $\Gamma_d\overline{\mathbf{Q}}\Gamma_d^{\mathrm{T}}$, where Γ_d represents the influence matrix associated with the unknown restoring force, $\mathbf{f}_d$, from the CBIS. In these simulations, the $\overline{\mathbf{Q}}$ matrix is set to $\overline{\mathbf{Q}} = 10^2\mathbf{I}_{4\times4}$, which results in an equivalent covariance matrix $\Gamma_d\overline{\mathbf{Q}}\Gamma_d^{\mathrm{T}}$ with an order of magnitude of 10^{-6}.

The forgetting factor ρ, $0 < \rho \leq 1$, is determined through trial-and-error to ensure the convergence of both the estimated responses and unknown restoring forces. The simulation results indicate that a ρ value in the range of 0.1 to 0.7 enables the KF-RLS to accurately estimate these quantities. Figures 7(a)–7(f) show the estimations for the second and fourth floors, as determined by AEKF (Case 1) and KF-RLS (Case 2). The results, when compared with the ground truth, validate the strong tracking performance of both the AEKF and KF-RLS algorithms.

5. System Identification of a Steel Frame Equipped with a CBIS

In this section, a series of experiments are conducted, including free vibration tests and shaking table tests. Then, the proposed technique is utilized for system identification and parameter analysis of the SDOF structure equipped with a CBIS.

5.1. Experimental Equipment. The experimental model consists of an SDOF steel frame as the primary structure and the CBIS. Three types of sensors are installed to measure structural responses. As illustrated in Figure 8(a), an accelerometer is installed on the top floor of the steel frame to measure the floor's acceleration. A displacement meter is used to measure the displacement of the top floor. Furthermore, two force sensors are installed in the steel cables to measure the tension of these cables.

The total height of the SDOF structure is 1 m. The top plate consists of steel plates (Q245) with plane dimensions of 0.834×0.39 m and a thickness of 0.01 m. Different dimensions of columns are adopted, respectively, in the cases of free vibration tests and shaking table tests. For the free vibration tests, the columns consist of steel plates (Q245) with height × width × thickness dimensions of $1 \times 0.15 \times 0.003$ m. The total mass of the primary structure is

Table 1: Comparison of identified parameters using AEKF and EKF.

Parameters		Actual	AEKF		EKF	
			Identified	Error (%)	Identified	Error (%)
Stiffness of the structure (N/m)	k_1	15000	14972	0.19	15026	0.17
	k_2	15000	14970	0.20	14973	0.18
	k_3	15000	14970	0.20	14941	0.39
	k_4	15000	14976	0.16	14924	0.51
Damping of the structure	α	0.3	0.3047	0.47	0.3009	0.30
	β	0.0025	0.0024	4.00	0.008	220.0
Damping of the CBIS (N/m/s)	c_{d1}	20	20.83	4.15	−68.17	440.9
	c_{d2}	20	21.53	7.65	−60.54	402.7
	c_{d3}	20	20.46	2.30	−59.04	395.2
	c_{d4}	20	21.88	9.40	−62.42	412.1

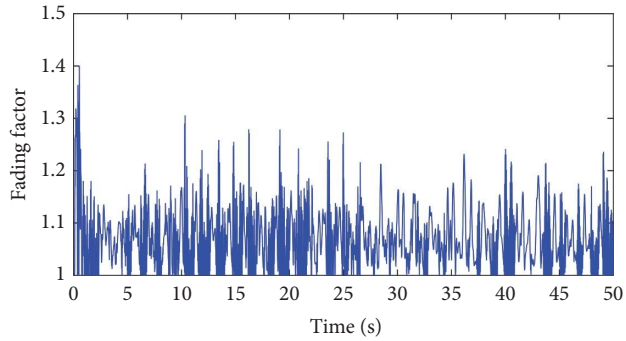

Figure 5: Time-variant fading factor in the AEKF.

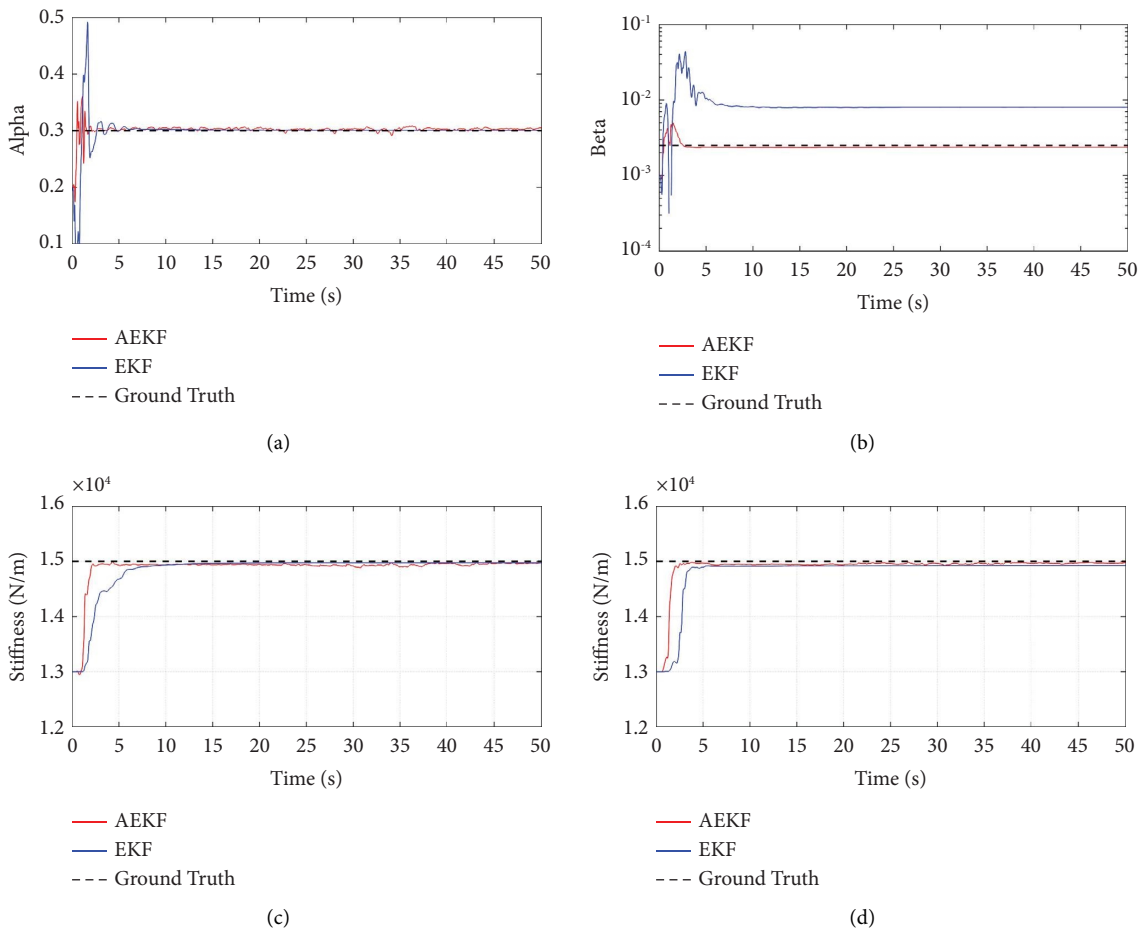

Figure 6: Continued.

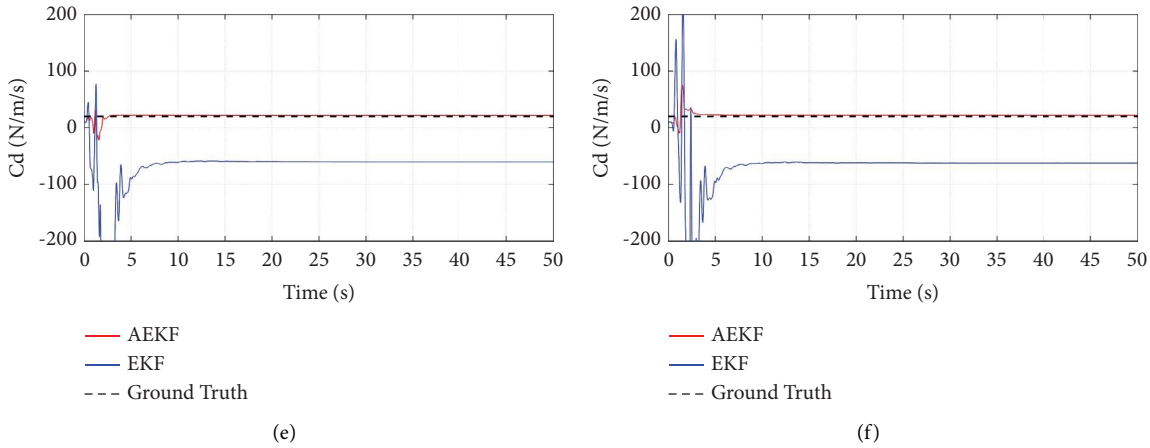

Figure 6: Comparison of the ground truth with estimated parameters from AEKF and EKF: (a) α, (b) β, (c) k_2, (d) k_4, (e) c_{d2}, and (f) c_{d4}.

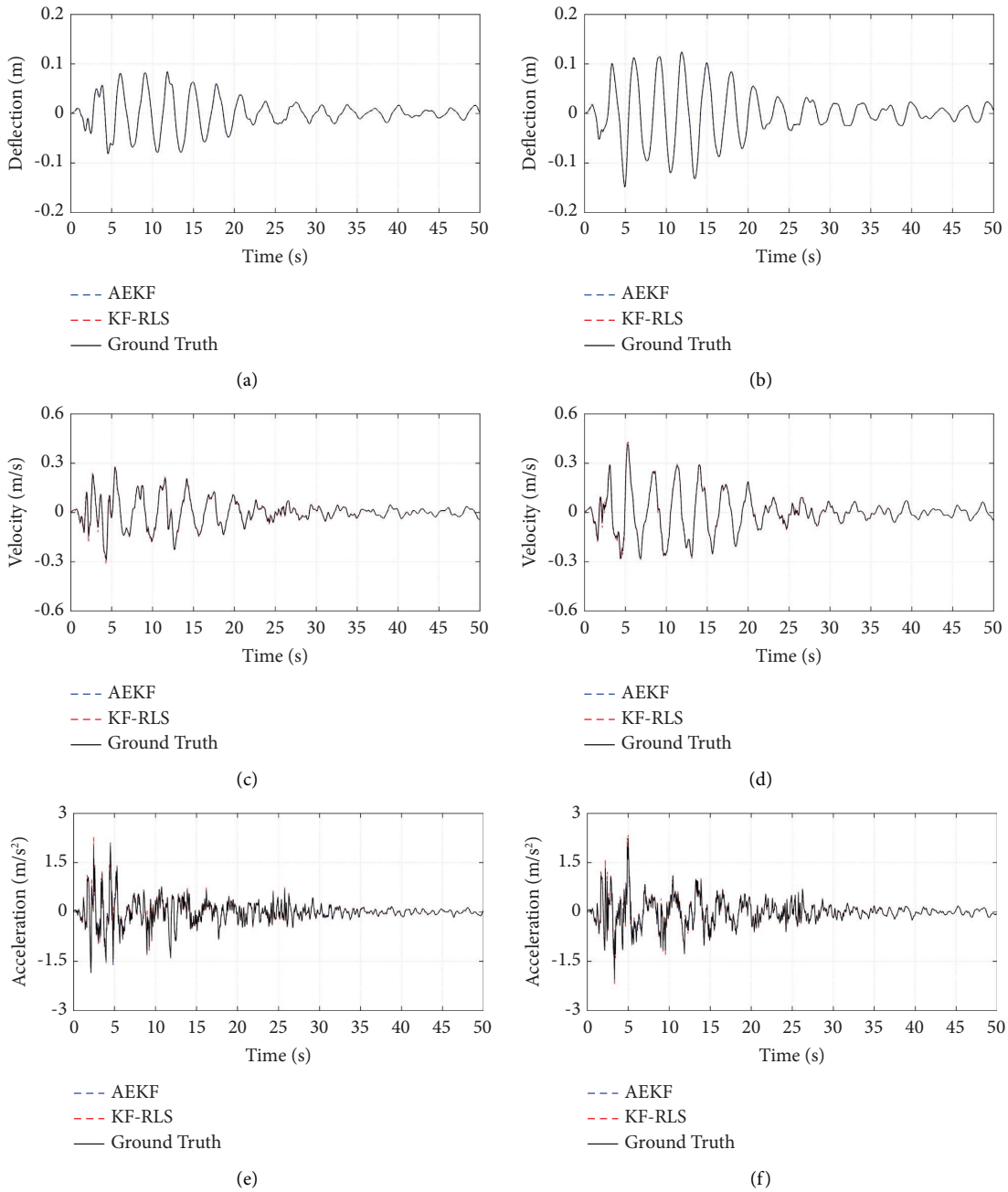

Figure 7: Continued.

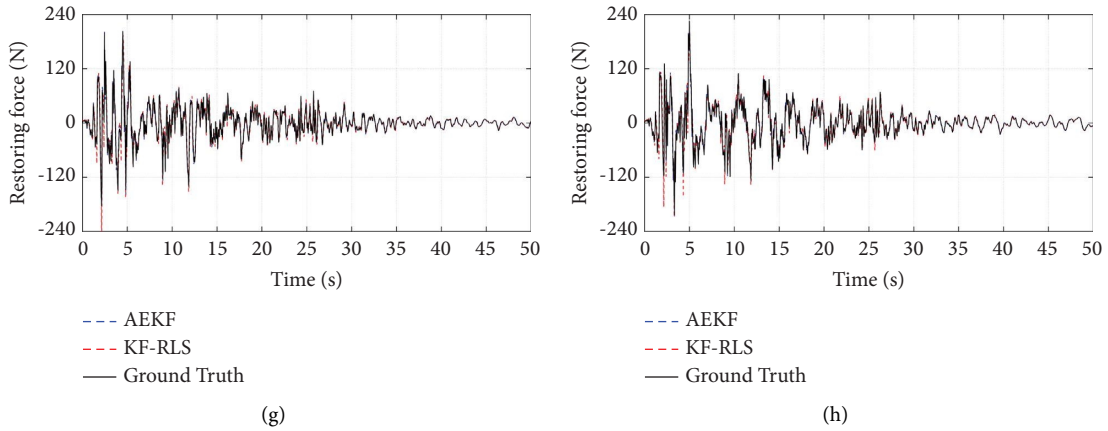

Figure 7: Comparison of the ground truth and the estimated response using AEKF (case 1) and KF-RLS (case 2): (a, b) deflection, (c, d) velocity, (e, f) acceleration, and (g, h) restoring force generated by the CBIS of second and fourth floors.

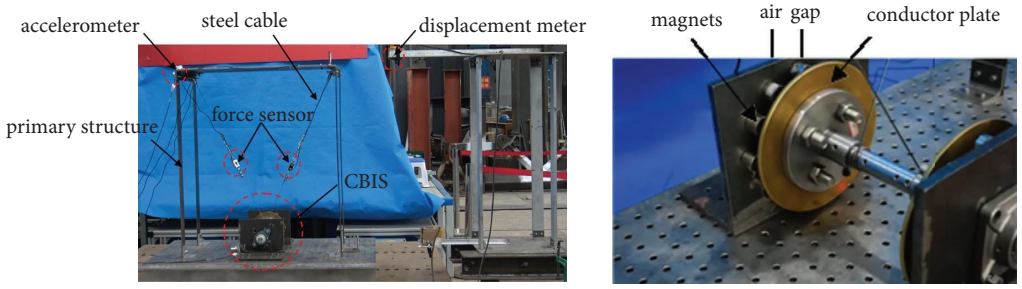

Figure 8: (a) Configuration of the test specimen and (b) details of CBIS.

23.0 kg, and the first natural frequency of the primary structure is adjusted to approximately 1 Hz. For the shaking table tests, a substantial reinforcement of the test frame is used to effectively simulate real-world seismic conditions. This led to increasing the column thickness from 3 mm to 5 mm, with the total mass being augmented to 26.6 kg. As a result, the natural frequency was tuned to approximately 2 Hz to ensure a resilient response to the higher intensity excitations envisaged in these tests. This adjustment was primarily to prevent plastic deformation under the rigorous demands of seismic wave excitations.

Figure 8(b) illustrates the details of the CBIS. Copper with high electrical conductivity is selected as the material for the rotating conducting plate. The supporting roller shaft is fabricated from steel, primarily serving a structural role by providing stability and support to the copper conducting plate. Although steel can engage in the electromagnetic dynamics of the system to a smaller extent, its use here is fundamentally for mechanical strength rather than for enhancing the eddy current effect. These magnets that are absorbed on the fixed side plates are cylindrical neodymium alloy (NdFeB) permanent magnets, each having a diameter of 25 mm and a thickness of 20 mm. It is worth noting that the magnetic poles are staggered according to the principle of opposite poles being present in adjacent magnets, adhering to a precise arrangement to maintain the functionality and efficacy of the system.

Various test conditions are designed to evaluate the performance of the CBIS, which can be seen in Table 2. The thickness of the rotating conducting plate of the CBIS is set as 5, 10, or 20 mm. If there are no magnets on the fixed side plates, the system can only function as an inerter without eddy current effects. In this case, the test conditions are labeled as "Md5," "Md10," or "Md20," corresponding to the thickness of the rotating conducting plate. However, if magnets are present on the fixed side plates, eddy currents can be generated when relative motion occurs between the rotating conductor plates and the magnets. The damping force induced by the eddy current effect varies by adjusting the air gap between the magnets and the conducting plate. For instance, the test condition is donated as "Md5-Cd10" when the thickness of the rotating conducting plate is 5 mm, and the air gap between the magnets and the conducting plate is set as 10 mm.

5.2. Free Vibration Tests. During the free vibration tests, the initial displacement of the top floor of the steel frame is set to 50 mm. The free vibration tests for the primary structure are first tested without a CBIS, followed by the tests with a CBIS.

5.2.1. Parameters Identification of the SDOF Structure without a CBIS. The equation of motion of the SDOF structure without a CBIS under free vibration can be

Table 2: Test conditions of the SDOF structure equipped with a CBIS.

Test conditions		Description	
		Thickness of rotating conducting plate (mm)	Air gap between the magnets and rotating conducting plate (mm)
Free vibration tests	Md5	5	No magnets
	Md5-Cd10	5	10
	Md5-Cd20	5	20
	Md5-Cd30	5	30
	Md5-Cd40	5	40
	Md10	10	No magnets
	Md10-Cd10	10	10
Shaking table tests	Md5	5	No magnets
	Md5-Cd10	5	10
	Md20	20	No magnets
	Md20-Cd10	20	10

expressed as $m\ddot{x} + c\dot{x} + kx = 0$, where $m = 23$ kg, the k and c denote the shear stiffness and damping coefficient of the primary structure without a CBIS, respectively. The goal is to identify the unknown parameters k and c, using the acceleration of the top floor from the accelerometer as the input. The displacement response of the top floor both in the time and frequency domains can be seen in Figures 9(a) and 9(b), respectively.

The damping ratio ξ can be calculated using the logarithmic decrement method:

$$\xi = \frac{1}{2\pi n} \ln \frac{x_k}{x_{k+n}}, \tag{37}$$

where x_k and x_{k+n} are displacement response amplitudes within n cycle intervals. From Figure 9(a), the damping ratio is calculated as $\xi = 0.33\%$. From Figure 9(b), the natural frequency of the structure can be calculated as 0.915 Hz by using the fast Fourier transform.

To identify the parameters and responses, the extended state vector can be represented as follows:

$$\begin{aligned} \dot{\mathbf{z}} &= \begin{Bmatrix} \dot{x} \\ \ddot{x} \\ \dot{c} \\ \dot{k} \end{Bmatrix} \\ &= \begin{Bmatrix} \dot{x} \\ m^{-1}(-c\dot{x} - kx) \\ 0 \\ 0 \end{Bmatrix}. \end{aligned} \tag{38}$$

The initial values used in the AEKF are given as follows: sampling interval $\Delta t = 0.001\,s$, the initial state vector $\mathbf{z} = \{0 \;\; 0 \;\; 1 \;\; 1000\}^T$, and the initial error covariance matrix $\mathbf{P} = 10^6 \mathbf{I}_{4\times 4}$. In laboratory tests, noise levels are typically more variable than in the controlled environment of numerical simulations, which are preset at a 5% level. This variability stems from factors such as environmental conditions, equipment quality, and operational precision. Consequently, a 5% noise level in the measurements is assumed, and the covariance matrix of measurement noise is derived as $\mathbf{R} = (5\% \times \mathrm{RMS}(\mathbf{Y}))^2 \approx 10^{-2}$.

Regarding the $\mathbf{Q}$ matrix, values smaller than 10^{-5} have been found to yield satisfactory results within numerical simulations that maintain controlled noise levels. In contrast, laboratory conditions characterized by less defined noise levels and potential data discrepancies require the adoption of smaller $\mathbf{Q}$ values for laboratory experiments. When deflection is used as the measurement input for AEKF, a $\mathbf{Q}$ value smaller than 10^{-5} is found to provide satisfactory results. However, for acceleration measurements, which are typically noisier and less smooth, a much smaller $\mathbf{Q}$ value of 10^{-11} is selected when the acceleration is used as the measurement input for AEKF to obtain more accurate estimations despite the presence of higher noise levels.

As shown in Figures 10(a) and 10(b), the shear stiffness k and damping coefficient c of the primary structure without a CBIS are estimated as $k = 756.57$ N/m and $c = 0.903$ Ns/m, respectively, and the corresponding estimated natural frequency and damping ratio are calculated as 0.913 Hz and 0.34%, respectively. The estimations based on AEKF are comparatively consistent with the calculated natural frequency and damping ratio. Figures 11(a) and 11(b) show the comparison results of the measured and estimated acceleration and deflection of the top floor, respectively. The estimated and measured results are in good agreement, suggesting the proposed technique can accurately estimate the unknown parameters and responses.

5.2.2. Identification of the Restoring Force Generated by the CBIS. After identifying the parameters of the primary structure without a CBIS, the free vibration test of the SDOF structure with a CBIS is then conducted. The equation of motion of the SDOF structure with a CBIS is expressed as equation (6). The experimental restoring force generated by the CBIS is calculated as the tension force difference between measurements of the two steel cables' tension. In order to identify the restoring force generated by the CBIS, two case

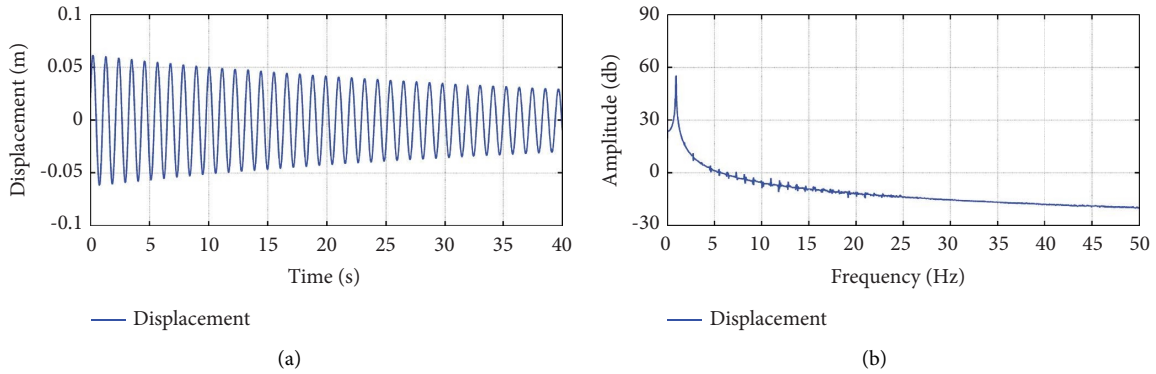

Figure 9: Displacement response at the roof of the frame without a CBIS: (a) time domain and (b) frequency domain.

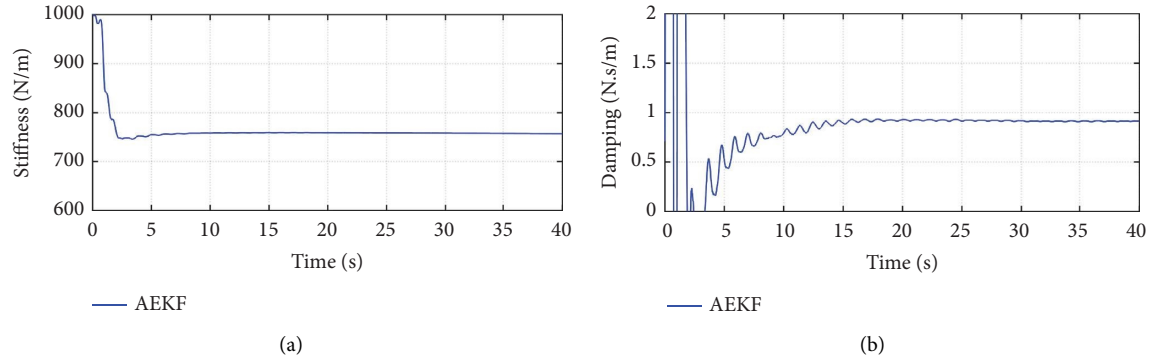

Figure 10: Parameter estimation of the frame without a CBIS (free vibration tests): (a) stiffness and (b) damping coefficient.

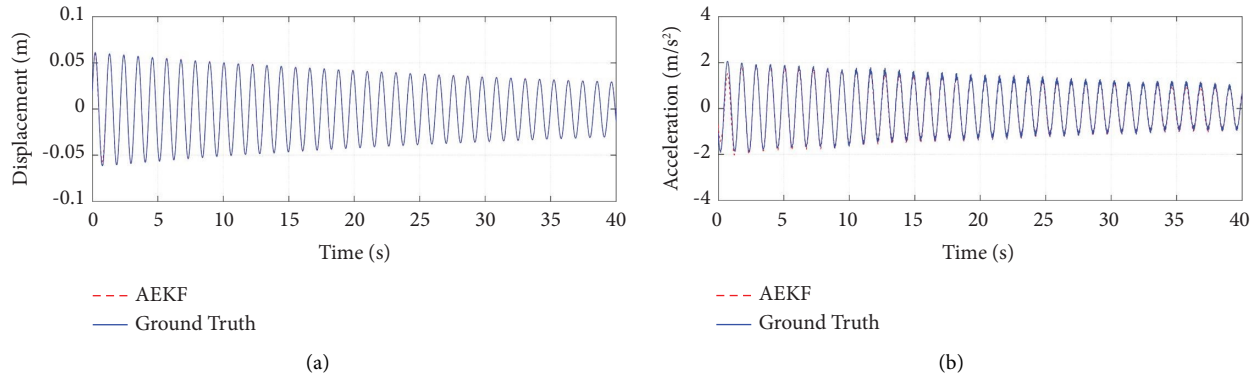

Figure 11: Response estimation at the roof of the frame without a CBIS (free vibration tests): (a) displacement and (b) acceleration.

studies are presented depending on the availability of the model of the CBIS.

For the first case in which the model of the CBIS is specific, the equivalent eddy current damping coefficient c_d of the CBIS is identified using the AEKF. The input for the identification is the acceleration response of the top floor. The initial values used in the AEKF are given as follows: sampling interval $\Delta t = 0.001\,s$, the covariance matrix of measurement noise is assumed as $\mathbf{R} = (5\% \times \mathrm{RMS}(\mathbf{Y}))^2 \approx 10^{-2}$, the covariance matrix of process noise $\mathbf{Q} = 10^{-11}\mathbf{I}_{3\times3}$, the initial state vector $\mathbf{z} = \{0\ \ 0\ \ 10\}^{\mathrm{T}}$, and the initial error covariance matrix $\mathbf{P} = 10^{6}\mathbf{I}_{3\times3}$. The calculated m_d and the identified c_d are summarized in Table 3. Then, the restoring force generated by the CBIS is calculated by $f_d = m_d\ddot{x} + c_d\dot{x}$.

For the second case in which the model of CBIS is assumed to be unspecific, thus the restoring force generated by the CBIS is identified by KF-RLS. The input for the identification is the displacement response of the top floor. The initial values used in the KF-RLS are given as follows:

Table 3: Calculated inertance and identified equivalent damping coefficient of the CBIS (free vibration tests).

Parameter	Md5-Cd40	Md5-Cd30	Md5-Cd20	Md5-Cd10	Md10-Cd10
m_d (kg)	11.73	11.73	11.73	11.73	23.45
c_d (Ns/m)	30.81	33.88	39.45	48.20	74.54

sampling interval $\Delta t = 0.001\,s$, the covariance matrix of measurement noise is assumed as $\overline{\mathbf{R}} = (5\% \times \mathrm{RMS}(\mathbf{Y}))^2 = 10^{-8}$, the covariance matrix of process noise $\overline{\mathbf{Q}} = 1$, the equivalent covariance matrix $\Gamma_d \overline{\mathbf{Q}} \Gamma_d^{\mathrm{T}}$ has a magnitude of 10^{-8}, the forgetting factor $\rho = 0.9$, and the initial values of the matrices are $\mathbf{P}_{k,0} = 10^{10}$, $\mathbf{P}^*_{k,0} = 10^{10}$, and $\mathbf{M}_{k,0} = \mathbf{0}_{2\times 2}$, respectively.

Figures 12(a) and 12(b) show the comparison results of the measured responses (blue solid line) and estimated responses (red dotted line) of displacement and acceleration of the top floor using two different strategies, respectively. It can be seen that the proposed technique effectively tracks the ground truth, as demonstrated by the close match between the estimations and measurements.

In addition, increasing the thickness of the rotating conductor plates increases from 5 mm (Md5) to 10 mm (Md10) which enhances the inertial and the damping effects provided by the CBIS increase, resulting in faster vibration attenuation. Likewise, reducing the air gap between the rotating conducting plate and the magnets from 40 mm (Cd40) to 10 mm (Cd10) improves the CBIS's damping effects, facilitating quicker dissipation of the vibrational energy. These observations indicate that the CBIS effectively bolsters the damping capability of the structure, minimizing vibrations and optimizing overall structural performance.

The comparison of the estimation and measurement of restoring force time history is plotted in Figure 13. As can be seen from the above plots, the restoring force generated by the CBIS can be identified with high accuracy for both cases using AEKF or KF-RLS.

5.3. Shaking Table Tests. For shaking table tests, three ground motions are utilized: EI Centro (1940, NS), Japan 311 wave (2011, NS), and Shanghai artificial wave (SHW, 1996). Each type of seismic wave acts along only one direction, and the peak value of the acceleration increases gradually from 0.1 to 0.3 g.

5.3.1. Parameters Identification of the SDOF Structure without a CBIS. The equation of motion for the SDOF structure without a CBIS under shaking table tests can be expressed as $m\ddot{x} + c\dot{x} + kx = -ma_g$, where $m = 26.6\,\mathrm{kg}$, a_g is the acceleration of the ground motion. The unknown parameters to be identified are k and c. The input for the identification here is the acceleration of the top floor from the accelerometer.

To identify the parameters and responses, the extended state vector can be represented as follows:

$$\dot{\mathbf{z}} = \begin{Bmatrix} \dot{x} \\ \ddot{x} \\ \dot{c} \\ \dot{k} \end{Bmatrix} = \begin{Bmatrix} \dot{x} \\ -m^{-1}(c\dot{x} + kx) - a_g \\ 0 \\ 0 \end{Bmatrix}. \tag{39}$$

The initial values used in the AEKF are given as follows: sampling interval $\Delta t = 0.001\,s$, the covariance matrix of measurement noise is assumed as $\mathbf{R} = (5\% \times \mathrm{RMS}(\mathbf{Y}))^2 \approx 10^{-2}$, the covariance matrix of process noise $\mathbf{Q} = 10^{-11}\mathbf{I}_{4\times 4}$, the initial state vector $\mathbf{z} = \{0 \;\; 0 \;\; 1 \;\; 1000\}^{\mathrm{T}}$, and the initial error covariance matrix $\mathbf{P} = 10^6 \mathbf{I}_{4\times 4}$.

Based on the assessment, the estimated parameters of the primary frame without a CBIS under different conditions are summarized in Table 4. The estimated stiffness is stable at around 4800 N/m, while the estimated damping coefficient ranges from 0.16% to 0.38% with an average of 0.25%. However, the standard extended Kalman filter without adaptive fading factors cannot identify the structural parameters and responses based on the experimental data from shaking table tests.

Figures 14 and 15 show the estimation of unknown parameters and responses of the SDOF structure without a CBIS under the SHW seismic excitation with a peak ground acceleration of 0.3 g. As shown in these figures, after an initial two-second period of fluctuation while searching for the true values, the estimated structural parameters and responses converge accurately to stable estimated values and measured structural responses, respectively. This demonstrates the effectiveness of the estimation method in determining the parameters and responses of the SDOF structure without a CBIS under seismic excitation.

5.3.2. Identification of the Restoring Force Generated by the CBIS. After identifying the parameters of the primary structure without a CBIS, shaking table tests of the SDOF structure with a CBIS were conducted. In line with the free vibration tests, two case studies are presented to identify the restoring force generated by the CBIS. For the first case, utilizing a specific CBIS model, the m_d of the CBIS is calculated and the c_d of the CBIS is identified using the AEKF. The input for the identification is the acceleration response of the top floor. The initial values used in the AEKF are given

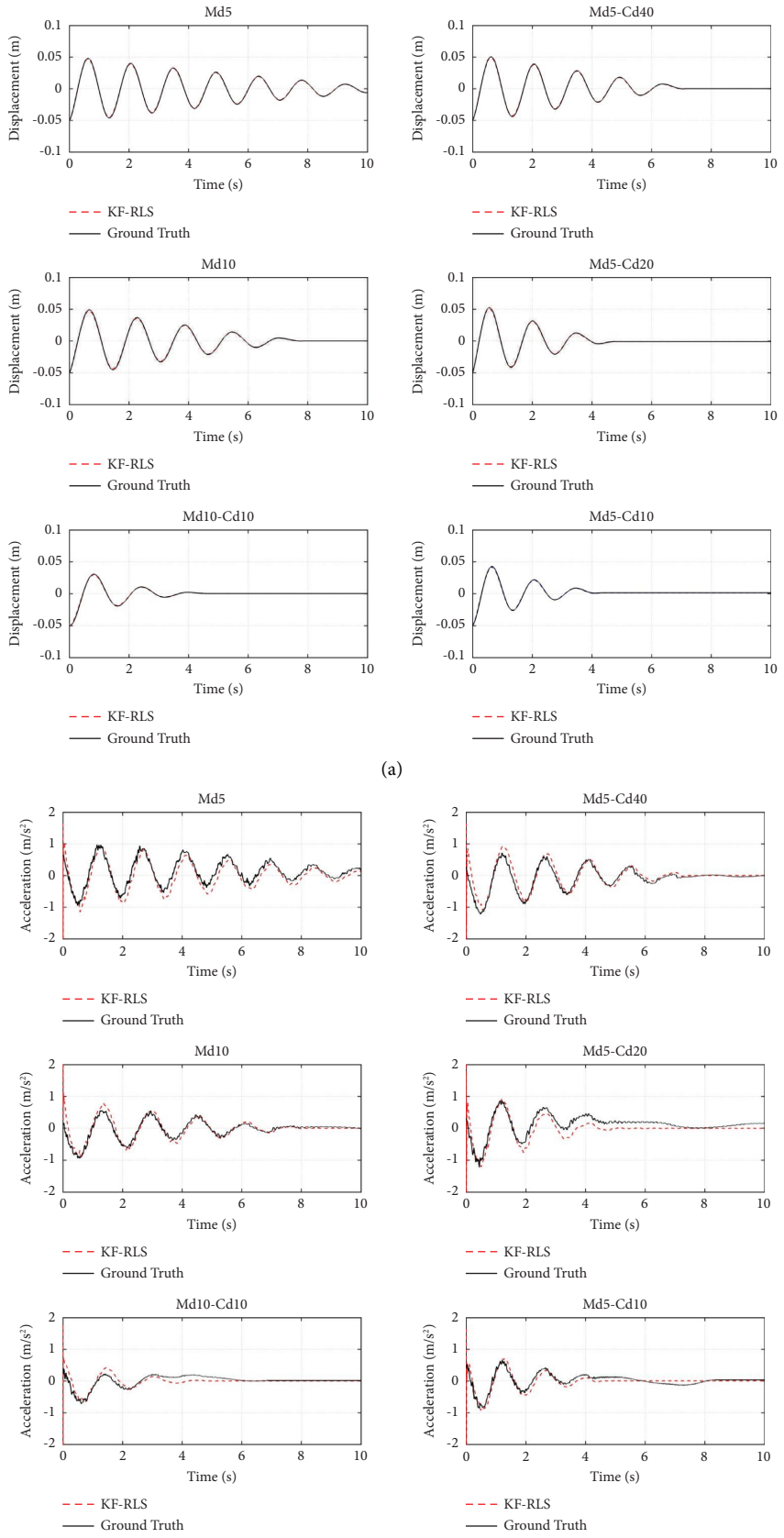

FIGURE 12: Response estimations of the frame with a CBIS: (a) displacement and (b) acceleration.

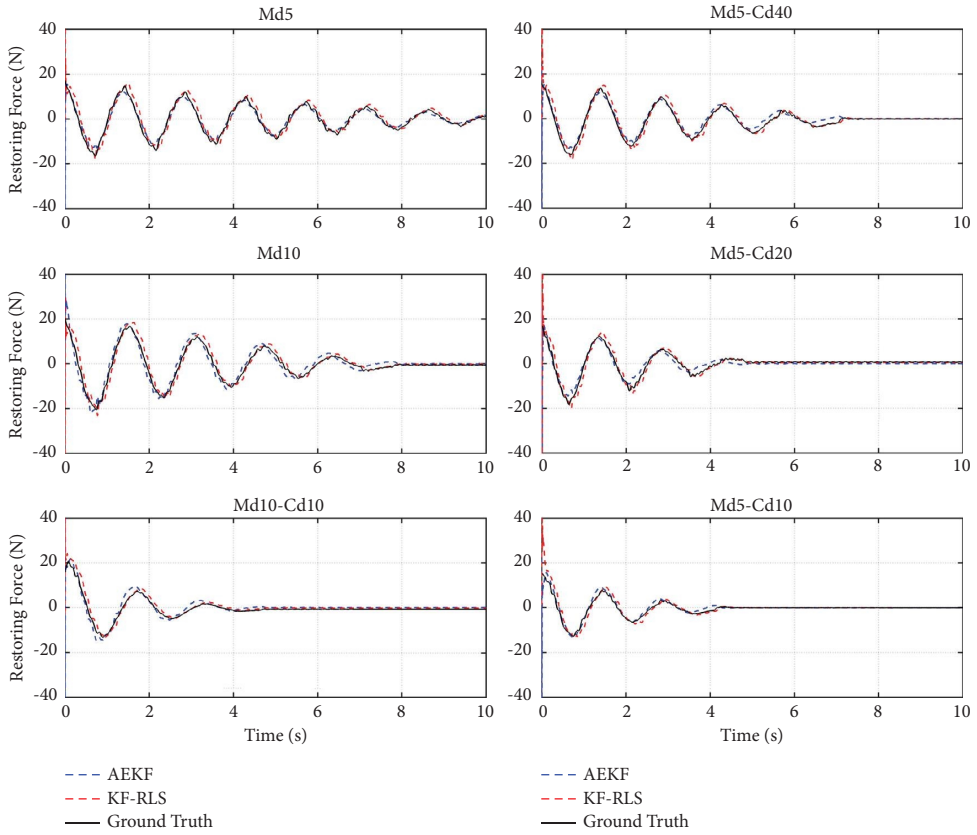

Figure 13: Comparison of the ground truth and the estimated restoring forces (free vibration tests) generated by the CBIS using AEKF (case 1) and KF-RLS (case 2), respectively.

Table 4: Parameter estimation of the primary frame without a CBIS (shaking table tests).

Seismic input		Stiffness (N/m)	Natural frequency (Hz)	Damping coefficient (Ns/m)	Damping ratio (%)
EI centro	0.1 g	4791.4	2.1360	1.5527	0.22
	0.2 g	4836.3	2.1460	2.2452	0.31
	0.3 g	4897.2	2.1595	2.7326	0.38
Japan 311	0.1 g	4822.7	2.1430	1.1643	0.16
	0.2 g	4811.4	2.1405	1.5321	0.21
	0.3 g	4780.0	2.1335	1.8370	0.26
SHW	0.1 g	4802.3	2.1385	1.6613	0.23
	0.2 g	4795.6	2.1370	1.8090	0.25
	0.3 g	4798.5	2.1376	2.0279	0.28

as follows: sampling interval $\Delta t = 0.001\,s$, the covariance matrix of measurement noise $\mathbf{R} = (5\% \times \mathrm{RMS}(\mathbf{Y}))^2 \approx 10^{-2}$, the covariance matrix of process noise $\mathbf{Q} = 10^{-11}\mathbf{I}_{4\times4}$, the initial state vector $\mathbf{z} = \{0\ \ 0\ \ 1000\}^{\mathrm{T}}$, and the initial error covariance matrix $\mathbf{P} = 10^{6}\mathbf{I}_{3\times3}$. The calculated m_d and identified c_d are summarized in Table 5. The restoring force by the CBIS is calculated by $f_d = m_d\ddot{x} + c_d\dot{x}$.

For the second case that the CBIS model is unspecific, the restoring force generated by the CBIS is identified by the KF-RSL. The input for the identification is the displacement response of the top floor. The initial values used in the KF-RSL are given as follows: sampling interval $\Delta t = 0.001\,s$, the covariance matrix of measurement noise $\overline{\mathbf{R}} = (5\% \times \mathrm{RMS}(\mathbf{Y}))^2 = 10^{-8}$, the covariance matrix of process noise $\overline{\mathbf{Q}} = 1$, the equivalent covariance matrix $\Gamma_d\overline{\mathbf{Q}}\Gamma_d^{\mathrm{T}}$ has a magnitude of 10^{-8}, the forgetting factor $\rho = 0.9$, and the initial values of the matrices are $\mathbf{P}_{k,0} = 10^{10}$, $\mathbf{P}^*_{k,0} = 10^{10}$, and $\mathbf{M}_{k,0} = \mathbf{0}_{2\times2}$, respectively. Utilizing the proposed technique, the structural response and the restoring force generated by the CBIS were then identified.

For instance, Figures 16 and 17 illustrate the estimated responses of the SDOF structure equipped with a CBIS (Md5) and the restoring force generated by the CBIS (Md5), respectively, under SHW seismic excitation with a peak

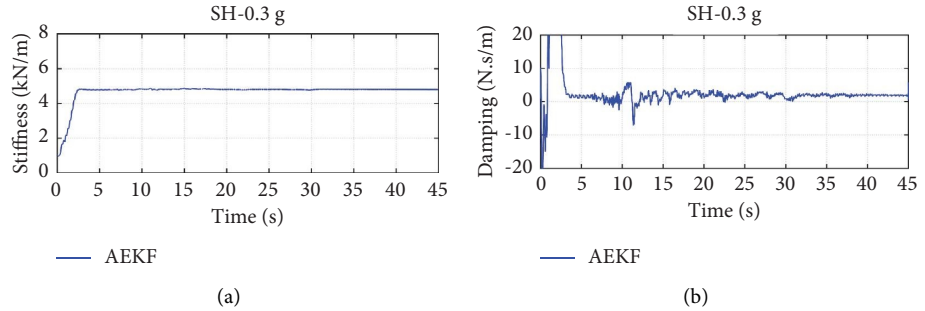

Figure 14: Parameter estimation of the frame without a CBIS (shaking table tests: SH-0.3 g): (a) stiffness and (b) damping coefficient.

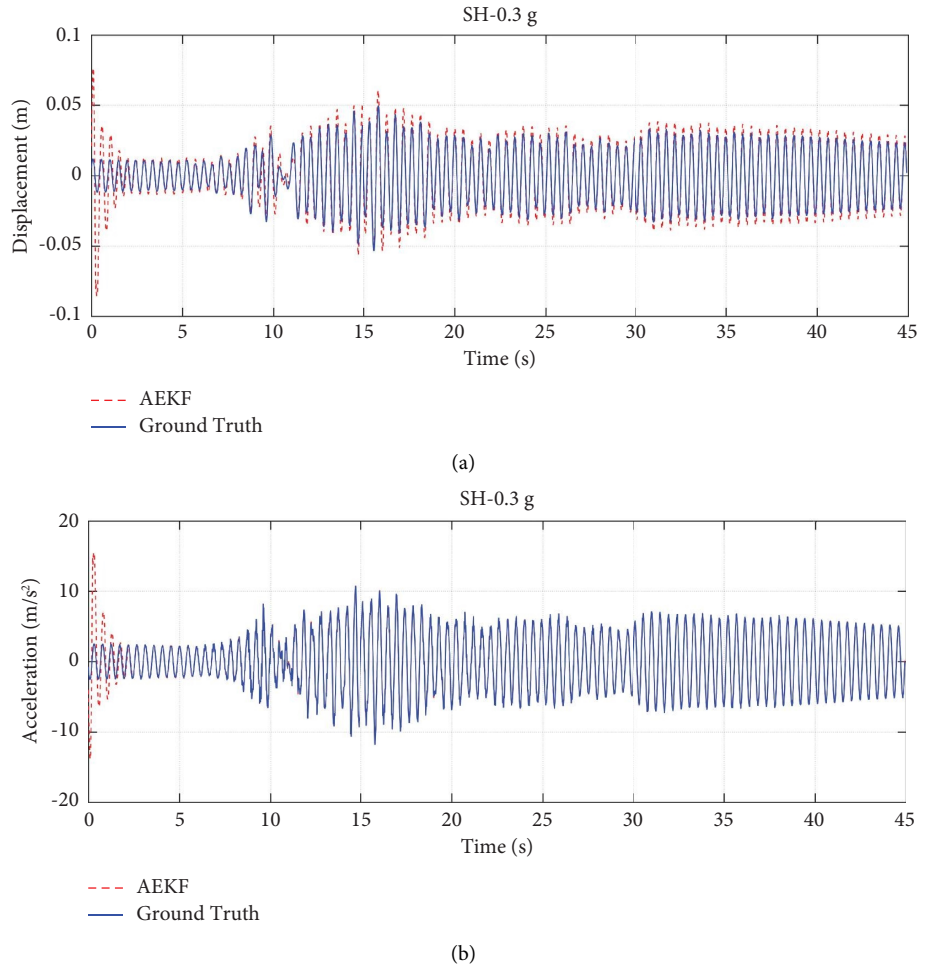

Figure 15: Response estimation at the roof of the frame without a CBIS using AEKF (shaking table tests: SH-0.3 g): (a) deflection and (b) acceleration.

ground acceleration of 0.3 g for both cases. The estimated responses of the top floor are in good agreement with the measured responses, as shown in Figures 16(a) and 16(b). Due to the intense vibration of steel cables during the shaking table tests, the force sensors in the steel cables have not obtained reliable data. Consequently, the estimated restoring forces provided by the CBIS under various seismic waves in two cases are presented in Figure 17. The results for two different cases align well with each other; however, they could not be validated through comparison with measurements in this paper.

5.4. Characteristics of the CBIS. The restoring force generated by the CBIS includes the inertia force and the eddy current damping force. This section aims to further study the characteristics of the CBIS and verify the feasibility of the

Table 5: Calculated inertance and identified equivalent damping coefficient of the CBIS (shaking table tests).

Seismic input		Md5-Cd10		Md20-Cd10	
		m_d (kg)	c_d (Ns/m)	m_d (kg)	c_d (Ns/m)
EI centro	0.1 g	11.73	215.45	46.91	386.14
	0.2 g	11.73	199.86	46.91	394.99
	0.3 g	11.73	193.19	46.91	389.29
Japan 311	0.1 g	11.73	210.92	46.91	393.98
	0.2 g	11.73	185.64	46.91	395.64
	0.3 g	11.73	177.41	46.91	396.31
SHW	0.1 g	11.73	229.37	46.91	384.30
	0.2 g	11.73	208.63	46.91	386.80
	0.3 g	11.73	201.25	46.91	388.80

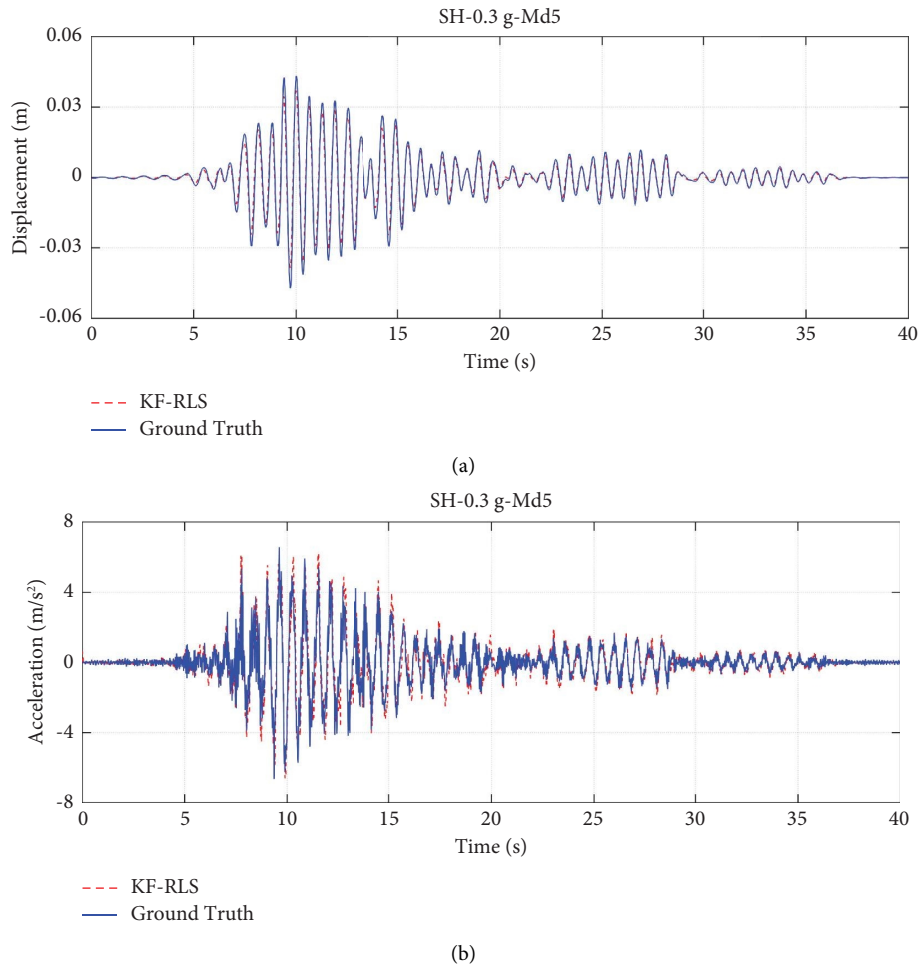

Figure 16: Response estimation at the roof of the frame with a CBIS using KF-RLS (shaking table tests: SH-0.3 g-Md5): (a) deflection and (b) acceleration.

mechanical model. The calculated inertance and identified equivalent damping coefficient of the CBIS for free vibration and shaking table tests are summarized in Tables 3 and 5, respectively. The air gap between the rotating conductor plates and magnets is a crucial parameter that influences the c_d of the CBIS. To examine the influence of the air gap on the damping performance of the CBIS, adjustments were made to the air gap while keeping the m_d constant. As shown in Table 3 and Figure 18, when the air gap increases from 10 mm to 40 mm, the c_d decreases from 48.20 to 30.81 Ns/m. This finding highlights the significance of the air gap in determining the damping performance of the CBIS.

The thickness of the rotating conductor plates plays a critical role in influencing both the inertial and the damping effect of the CBIS. As shown in Table 3, when the thickness of the rotating conductor plates increases from 5 mm to 10 mm, while maintaining the air gap at 10 mm, the m_d of the CBIS increases from 11.73 to 23.45 kg, and the c_d

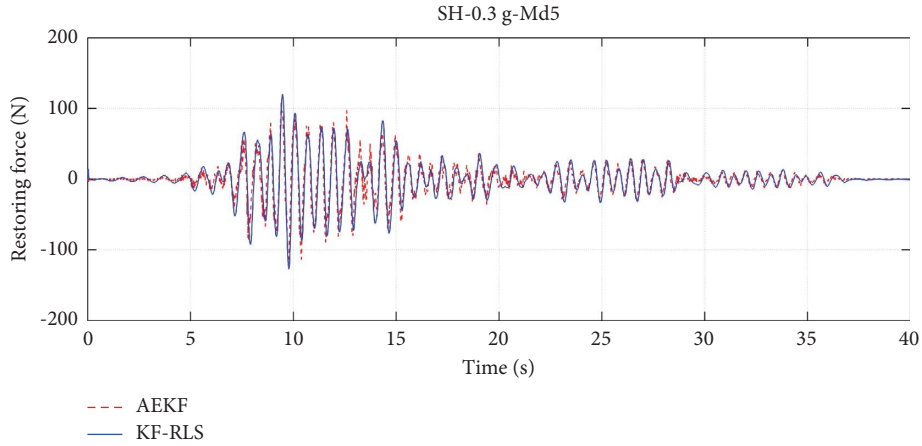

Figure 17: Comparison of the estimated restoring forces (SH-0.3 g-Md5) generated by the CBIS using AEKF (case 1) and KF-RLS (case 2).

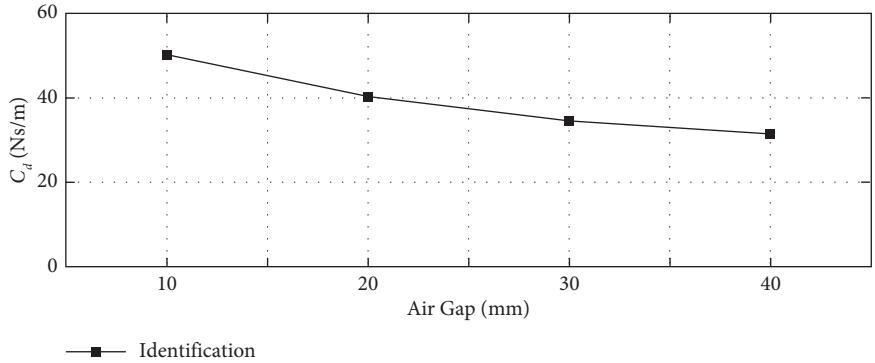

Figure 18: Effects of air gap on the eddy current damping coefficient of the CBIS.

increases from 48.20 to 74.54 Ns/m. Table 5 shows the results for shaking table tests, the c_d for Md5-Cd10 and Md20-Cd10 are almost 200 Ns/m and 400 Ns/m, respectively, for different types and amplitude levels of seismic waves. Again, the rotating conductor plate of the CBIS with a larger thickness will have a larger m_d and c_d. Moreover, the values of c_d of CBIS in shaking table tests are higher than those in free vibration tests. A possible explanation is that the steel frame equipped with a CBIS, when subjected to the seismic excitations in shaking table tests, experiences longer constant vibration. This allows the eddy current damping effect of the CBIS be fully realized, leading to a larger c_d value.

6. Conclusions

In this study, a comprehensive experimental program was conducted to evaluate the characteristics of an innovative cable-bracing inerter system (CBIS) by performing free vibration and shaking table tests on a one-story steel frame. A system identification approach, based on the adaptive extended Kalman filter (AEKF) and a recursive least-squares (RLS) algorithm, was developed and demonstrated to be highly accurate in identifying the structural parameters and the restoring force generated by the CBIS.

The results show that the CBIS provides substantial inertial and damping forces, thereby improving the dynamic performance of the steel frame. It was observed that the mass of the rotating conductor plates had a significant impact on the inertial and damping effects, with an increase in inertance and eddy current effect as the thickness of the plates increased. Furthermore, the study verified the influence of the air gap between the rotating conductor plates and magnets on the damping effect, with larger air gaps resulting in reduced damping effects in terms of the eddy current effect.

These findings not only validate the governing laws of the CBIS behavior in accordance with the proposed mechanical model but also highlight its effectiveness in achieving its intended functions. While additional research is needed to further investigate the operating principles and validate the estimated parameters of the CBIS, the CBIS has been proven to possess a robust and efficient energy dissipation mechanism and can provide substantial inertial and damping force. As a result, the CBIS holds immense potential for a wide range of applications in vibration control of buildings in civil engineering.

Appendix

A. Time-Variant Fading Factor

The time-variant fading factor λ_k is determined by solving anoptimization problem, equation (18). One sufficient condition of equation (18) is the covariance of innovation

residual sequences $E[\boldsymbol{\varepsilon}_{k+j}\boldsymbol{\varepsilon}_k^T] = 0$. To obtain an exact solution is challenging; however, it has been proved that [55, 56], if $O(|\boldsymbol{\varepsilon}_k|^2) \sqsubseteq O(|\boldsymbol{\varepsilon}_k|)$, the covariance of residual error sequences $E[\boldsymbol{\varepsilon}_{k+j}\boldsymbol{\varepsilon}_k^T]$ different times can be approximately expressed as:

$$E\left[\boldsymbol{\varepsilon}_{k+j}\boldsymbol{\varepsilon}_k^T\right] \approx \mathbf{H}_{k+j}\boldsymbol{\phi}_{k+j-1}\left(\mathbf{I} - \mathbf{K}_{k+j-1}\mathbf{H}_{k+j-1}\right)\cdots\boldsymbol{\phi}_{k+1}\left(\mathbf{I} - \mathbf{K}_{k+1}\mathbf{H}_{k+1}\right)\boldsymbol{\phi}_k\left(\widehat{\mathbf{P}}_k^- \mathbf{H}_k^T - \mathbf{K}_k\mathbf{V}_k\right), \tag{A.1}$$

where $\mathbf{V}_k$ is the covariance matrix of the estimated output error, $\mathbf{V}_k = E[\boldsymbol{\varepsilon}_k\boldsymbol{\varepsilon}_k^T]$. Therefore, the sufficient condition of the orthogonality is as follows:

$$\widehat{\mathbf{P}}_k^- \mathbf{H}_k^T - \mathbf{K}_k\mathbf{V}_k = 0. \tag{A.2}$$

Substituting the Kalman gain equation (18) into equation (A.2),

$$\widehat{\mathbf{P}}_k^- \mathbf{H}_k^T\left[\mathbf{I} - \left(\mathbf{H}_\mathbf{k}\widehat{\mathbf{P}}_k^- \mathbf{H}_k^T + \mathbf{R}_k\right)^{-1}\mathbf{V}_k\right] = 0. \tag{A.3}$$

Therefore, the sufficient condition of equation (A.3) is as follows:

$$\mathbf{H}_\mathbf{k}\widehat{\mathbf{P}}_k^- \mathbf{H}_k^T + \mathbf{R}_k = \mathbf{V}_k. \tag{A.4}$$

Substituting the error covariance matrix equation (14) into equation (A.4),

$$\mathbf{H}_\mathbf{k}\left(\lambda_k\boldsymbol{\phi}_{k-1}\widehat{\mathbf{P}}_{k-1}^+\boldsymbol{\phi}_{k-1}^T\right)\mathbf{H}_k^T + \mathbf{R}_k = \mathbf{V}_k. \tag{A.5}$$

Taking the trace on both sides of equation (A.5), a simple approximate solution for λ_k can be obtained and expressed as follows:

$$\lambda_{0,k} = \frac{tr\left[\mathbf{V}_k - \mathbf{H}_k\mathbf{Q}_{k-1}\mathbf{H}_k^\mathrm{T} - \mathbf{R}_k\right]}{tr\left[\mathbf{H}_k\boldsymbol{\Phi}_{k-1}\mathbf{P}_{k-1}^+\boldsymbol{\Phi}_{k-1}^\mathrm{T}\mathbf{H}_k^\mathrm{T}\right]}. \tag{A.6}$$

As λ_k should be no less than 1, a final expression for λ_k can be obtained as follows:

$$\lambda_k = \begin{cases} \lambda_{0,k}, & \lambda_{0,k} \geq 1, \\ 1, & \lambda_{0,k} < 1. \end{cases} \tag{A.7}$$

B. Recursive Relationship between Innovation Residual Sequences and the Unknown Restoring Force

As shown in equations (29) and (30), the posterior estimations of $\mathbf{Z}_k$ without and with $\mathbf{f}_d$ are donated as $\overline{\mathbf{Z}}_k^+$ and $\widehat{\mathbf{Z}}_k^+$, respectively. $\Delta\mathbf{Z}_k$ is the difference between $\overline{\mathbf{Z}}_k^+$ and $\widehat{\mathbf{Z}}_k^+$, which can be calculated as follows:

$$\begin{aligned}\Delta\mathbf{Z}_k &= \widehat{\mathbf{Z}}_k^+ - \overline{\mathbf{Z}}_k^+ = \widehat{\mathbf{Z}}_k^- - \overline{\mathbf{Z}}_k^- + \mathbf{H}_k\mathbf{K}_k\left(\overline{\mathbf{Z}}_k^- - \widehat{\mathbf{Z}}_k^-\right) \\ &= \left(1 - \mathbf{H}_k\mathbf{K}_k\right)\left(\widehat{\mathbf{Z}}_k^- - \overline{\mathbf{Z}}_k^-\right).\end{aligned} \tag{B.1}$$

Substituting equations (27) and (28) into equation (B.1),

$$\begin{aligned}\Delta\mathbf{Z}_k &= \left(\mathbf{I} - \mathbf{H}_k\mathbf{K}_k\right)\left(\widehat{\mathbf{Z}}_k^- - \overline{\mathbf{Z}}_k^-\right) \\ &= \left(\mathbf{I} - \mathbf{H}_k\mathbf{K}_k\right)\left(\mathbf{A}\widehat{\mathbf{Z}}_{k-1}^+ + \mathbf{B}\mathbf{f}_{k-1} + \mathbf{B}_d\mathbf{f}_{d,k-1} - \mathbf{A}\overline{\mathbf{Z}}_{k-1}^+ - \mathbf{B}\mathbf{f}_{k-1}\right) \\ &= \left(1 - \mathbf{H}_k\mathbf{K}_k\right)\left(\mathbf{A}\Delta\mathbf{Z}_{k-1} + \mathbf{B}_d\mathbf{f}_{d,k-1}\right).\end{aligned} \tag{B.2}$$

Let $\Delta\mathbf{Z}_k = \mathbf{M}_k\mathbf{B}_d\mathbf{f}_{d,k-1}$ and substituting it into equation (B.2), assuming that $\mathbf{f}_d$ is a constant over the certain interval, then $\mathbf{M}_k$ can be expressed as follows (or equation (33)):

$$\mathbf{M}_k = \left(\mathbf{I} - \mathbf{H}_k\mathbf{K}_k\right)\left(\mathbf{A}\mathbf{M}_{k-1} + \mathbf{I}\right). \tag{B.3}$$

$\overline{\mathbf{Y}}_k$ and $\widehat{\mathbf{Y}}_k$ are the innovation residual sequences without or with $\mathbf{f}_d$, respectively. $\Delta\mathbf{Y}_k$ is the difference between $\overline{\mathbf{Y}}_k$ and $\widehat{\mathbf{Y}}_k$, which can be expressed as follows:

$$\begin{aligned}\Delta\mathbf{Y}_k &= \overline{\mathbf{Y}}_k - \widehat{\mathbf{Y}}_k = \left(\mathbf{Y}_k - \mathbf{H}_k\overline{\mathbf{Z}}_k^-\right) - \left(\mathbf{Y}_k - \mathbf{H}_k\widehat{\mathbf{Z}}_k^-\right) \\ &= \mathbf{H}_k\left(\widehat{\mathbf{Z}}_k^- - \overline{\mathbf{Z}}_k^-\right).\end{aligned} \tag{B.4}$$

Substituting equations (25) and (26) and $\Delta\mathbf{Z}_k = \mathbf{M}_k\mathbf{B}_d\mathbf{f}_{d,k-1}$ into equation (B.4),

$$\begin{aligned}\Delta\mathbf{Y}_k &= \overline{\mathbf{Y}}_k - \widehat{\mathbf{Y}}_k = \mathbf{H}_k\left(\widehat{\mathbf{Z}}_k^- - \overline{\mathbf{Z}}_k^-\right) = \mathbf{H}_k\left(\mathbf{A}\Delta\mathbf{Z}_{k-1} + \mathbf{B}_d\mathbf{f}_{d,k-1}\right) \\ &= \mathbf{H}_k\left(\mathbf{A}\mathbf{M}_{k-1}\mathbf{B}_d\mathbf{f}_{d,k-2} + \mathbf{B}_d\mathbf{f}_{d,k-1}\right) \\ &= \mathbf{H}_k\left(\mathbf{A}\mathbf{M}_{k-1} + \mathbf{I}\right)\mathbf{B}_d\mathbf{f}_{d,k-1}.\end{aligned} \tag{B.5}$$

Therefore, the recursive relationship between $\overline{\mathbf{Y}}_k$, $\widehat{\mathbf{Y}}_k$, and the unknown $\mathbf{f}_d$ can expressed as follows (or equation (31)):

$$\overline{\mathbf{Y}}_k = \widehat{\mathbf{Y}}_k + \mathbf{B}_k\mathbf{f}_{d,k-1}, \tag{B.6}$$

where $\mathbf{B}_k$ is defined as the sensitivity matrix and calculated by the following equation (or equation (32)):

$$\mathbf{B}_k = \mathbf{H}_k\left(\mathbf{A}\mathbf{M}_{k-1} + \mathbf{I}\right)\mathbf{B}_d. \tag{B.7}$$

Data Availability

The data used to support the findings of this study are available from the corresponding author upon request.

Conflicts of Interest

The authors declare that they have no conflicts of interest.

Acknowledgments

The authors gratefully acknowledge the National Key R&D Program of China (Grant no. 2021YFE0112200), the Natural Science Foundation of Shanghai (Grant no. 20ZR1461800), and the Shanghai Pujiang Program (Grant no. 23PJ1421100) for having guided and funded the research presented in this article.

References

[1] O. El-Khoury and H. Adeli, "Recent advances on vibration control of structures under dynamic loading," *Archives of Computational Methods in Engineering*, vol. 20, no. 4, pp. 353–360, 2013.

[2] Z. R. Wani, M. Tantray, E. Noroozinejad Farsangi et al., "A critical review on control strategies for structural vibration control," *Annual Reviews in Control*, vol. 54, pp. 103–124, 2022.

[3] Q. Wu, H. Yan, H. Zhu, and X. Bai, "Shaking table test study on the seismic isolation effect of a hybrid passive control system," *Measurement*, vol. 164, Article ID 108125, 2020.

[4] M. Basili, M. De Angelis, and G. Fraraccio, "Shaking table experimentation on adjacent structures controlled by passive and semi-active MR dampers," *Journal of Sound and Vibration*, vol. 332, no. 13, pp. 3113–3133, 2013.

[5] N. Caterino, M. Spizzuoco, and A. Occhiuzzi, "Shaking table testing of a steel frame structure equipped with semi-active MR dampers: comparison of control algorithms," *Smart Structures and Systems*, vol. 15, no. 4, pp. 963–995, 2015.

[6] K. Kasai, A. Mita, H. Kitamura, K. Matsuda, T. A. Morgan, and A. W. Taylor, "Performance of seismic protection technologies during the 2011 Tohoku-Oki earthquake," *Earthquake Spectra*, vol. 29, no. 1_suppl, pp. 265–293, 2013.

[7] M. Cao, H. Tang, N. Funaki, and S. Xue, "Study on a real 8F steel building with oil damper damaged during the 2011 Great East Japan Earthquake," in *Proceedings of the 15th World Conference on Earthquake Engineering*, Lisbon, Portugal, September 2012.

[8] L. Xie, M. Cao, N. Funaki, H. Tang, and S. Xue, "Performance study of an eight-story steel building equipped with oil dampers damaged during the 2011 great east Japan earthquake part 1: structural identification and damage reasoning," *Journal of Asian Architecture and Building Engineering*, vol. 14, no. 1, pp. 181–188, 2015.

[9] M. Cao, L. Xie, H. Tang, N. Funaki, and S. Xue, "Performance study of an 8-story steel building equipped with oil damper damaged during the 2011 great east Japan earthquake Part 2: novel retrofit strategy," *Journal of Asian Architecture and Building Engineering*, vol. 15, no. 2, pp. 303–310, 2016.

[10] R. Ma, K. Bi, and H. Hao, "Inerter-based structural vibration control: a state-of-the-art review," *Engineering Structures*, vol. 243, Article ID 112655, 2021.

[11] M. C. Smith, "Synthesis of mechanical networks: the inerter," *IEEE Transactions on Automatic Control*, vol. 47, no. 10, pp. 1648–1662, 2002.

[12] K. Ikago, K. Saito, and N. Inoue, "Seismic control of single-degree-of-freedom structure using tuned viscous mass damper," *Earthquake Engineering & Structural Dynamics*, vol. 41, no. 3, pp. 453–474, 2012.

[13] L. Marian and A. Giaralis, "Optimal design of a novel tuned mass-damper–inerter (TMDI) passive vibration control configuration for stochastically support-excited structural systems," *Probabilistic Engineering Mechanics*, vol. 38, pp. 156–164, 2014.

[14] I. F. Lazar, S. A. Neild, and D. J. Wagg, "Using an inerter-based device for structural vibration suppression," *Earthquake Engineering & Structural Dynamics*, vol. 43, no. 8, pp. 1129–1147, 2014.

[15] D. Konstantinidis, N. Makris, and J. M. Kelly, "In-situ condition assessment of seismic fluid dampers: experimental studies and challenges," *Meccanica*, vol. 50, no. 2, pp. 323–340, 2015.

[16] H. A. Sodano, J. S. Bae, D. J. Inman, and W. Keith Belvin, "Concept and model of eddy current damper for vibration suppression of a beam," *Journal of Sound and Vibration*, vol. 288, no. 4-5, pp. 1177–1196, 2005.

[17] A. Tonoli, "Dynamic characteristics of eddy current dampers and couplers," *Journal of Sound and Vibration*, vol. 301, no. 3-5, pp. 576–591, 2007.

[18] K. Karakoc, A. Suleman, and E. J. Park, "Analytical modeling of eddy current brakes with the application of time varying magnetic fields," *Applied Mathematical Modelling*, vol. 40, no. 2, pp. 1168–1179, 2016.

[19] L. Irazu and M. J. Elejabarrieta, "Analysis and numerical modelling of eddy current damper for vibration problems," *Journal of Sound and Vibration*, vol. 426, pp. 75–89, 2018.

[20] X. Lu, Q. Zhang, W. Wu, and J. Shan, "Data-driven two-level performance evaluation of eddy-current tuned mass damper for building structures using shaking table and field testing," *Computer-Aided Civil and Infrastructure Engineering*, vol. 34, no. 1, pp. 38–57, 2019.

[21] S. Liu, Z. Lu, P. Li, S. Ding, and F. Wan, "Shaking table test and numerical simulation of eddy-current tuned mass damper for structural seismic control considering soil-structure interaction," *Engineering Structures*, vol. 212, Article ID 110531, 2020.

[22] M. Liu, S. Li, T. Wu, Y. Li, H. Meng, and Z. Chen, "Eddy-current tuned mass dampers for mitigation of wind-induced response of the noor III solar tower: design, installation, and validation," *Journal of Structural Engineering*, vol. 147, no. 12, Article ID 05021009, 2021.

[23] J. S. Hwang, J. Kim, and Y. Kim, "Rotational inertia dampers with toggle bracing for vibration control of a building structure," *Engineering Structures*, vol. 29, no. 6, pp. 1201–1208, 2007.

[24] S. Sorace and G. Terenzi, "The damped cable system for seismic protection of frame structures- Part I: general concepts, testing and modeling," *Earthquake Engineering & Structural Dynamics*, vol. 41, no. 5, pp. 915–928, 2012.

[25] S. Sorace and G. Terenzi, "The damped cable system for seismic protection of frame structures- Part II: design and application," *Earthquake Engineering & Structural Dynamics*, vol. 41, no. 5, pp. 929–947, 2012.

[26] A. M. Aly, "The use of bracing systems with MR dampers in super tall buildings," *International Journal of High-Rise Buildings*, vol. 5, no. 1, pp. 31–41, 2016.

[27] L. Xie, X. Ban, S. Xue, K. Ikago, J. Kang, and H. Tang, "Theoretical study on a cable-bracing inerter system for seismic mitigation," *Applied Sciences*, vol. 9, no. 19, p. 4096, 2019.

[28] S. Xue, J. Kang, L. Xie, R. Zhang, and X. Ban, "Cross-layer installed cable-bracing inerter system for MDOF structure seismic response control," *Applied Sciences*, vol. 10, no. 17, p. 5914, 2020.

[29] J. Kang, S. Xue, L. Xie, H. Tang, and R. Zhang, "Multi-modal seismic control design for multi-storey buildings using cross-

layer installed cable-bracing inerter systems: Part 1 theoretical treatment," *Soil Dynamics and Earthquake Engineering*, vol. 164, Article ID 107639, 2023.

[30] G. Kerschen, K. Worden, A. F. Vakakis, and J. C. Golinval, "Past, present and future of nonlinear system identification in structural dynamics," *Mechanical Systems and Signal Processing*, vol. 20, no. 3, pp. 505–592, 2006.

[31] J. P. Noël and G. Kerschen, "Nonlinear system identification in structural dynamics: 10 more years of progress," *Mechanical Systems and Signal Processing*, vol. 83, pp. 2–35, 2017.

[32] Y. Lei, W. Hua, S. Luo, and M. He, "Detection and parametric identification of structural nonlinear restoring forces from partial measurements of structural responses," *Structural Engineering & Mechanics*, vol. 54, no. 2, pp. 291–304, 2015.

[33] L. Liu, Y. Lei, and M. He, "A two-stage parametric identification of strong nonlinear structural systems with incomplete response measurements," *International Journal of Structural Stability and Dynamics*, vol. 16, no. 04, Article ID 1640022, 2016.

[34] C. Jin, S. Jang, and X. Sun, "An integrated real-time structural damage detection method based on extended Kalman filter and dynamic statistical process control," *Advances in Structural Engineering*, vol. 20, no. 4, pp. 549–563, 2017.

[35] C. K. Ma, J. M. Chang, and D. C. Lin, "Input forces estimation of beam structures by an inverse method," *Journal of Sound and Vibration*, vol. 259, no. 2, pp. 387–407, 2003.

[36] E. Lourens, E. Reynders, G. De Roeck, G. Degrande, and G. Lombaert, "An augmented Kalman filter for force identification in structural dynamics," *Mechanical Systems and Signal Processing*, vol. 27, pp. 446–460, 2012.

[37] F. Naets, J. Cuadrado, and W. Desmet, "Stable force identification in structural dynamics using Kalman filtering and dummy-measurements," *Mechanical Systems and Signal Processing*, vol. 50-51, pp. 235–248, 2015.

[38] K. Maes, A. W. Smyth, G. De Roeck, and G. Lombaert, "Joint input-state estimation in structural dynamics," *Mechanical Systems and Signal Processing*, vol. 70-71, pp. 445–466, 2016.

[39] X. Zhang, J. He, and M. Qi, "Study on KF-based responses reconstruction of nonlinear structure and external excitation identification," *Journal of Building Structures*, vol. 41, no. 11, pp. 143–149, 2020.

[40] L. Liu, J. Zhu, Y. Su, and Y. lei, "Improved Kalman filter with unknown inputs based on data fusion of partial acceleration and displacement measurements," *Smart Structures and Systems*, vol. 17, no. 6, pp. 903–915, 2016.

[41] L. Liu, Y. Su, J. Zhu, and Y. Lei, "Data fusion based EKF-UI for real-time simultaneous identification of structural systems and unknown external inputs," *Measurement*, vol. 88, pp. 456–467, 2016.

[42] Y. Lei, S. J. Luo, and M. Y. He, "Identification of model-free structural nonlinear restoring forces using partial measurements of structural responses," *Advances in Structural Engineering*, vol. 20, no. 1, pp. 69–80, 2017.

[43] Y. Lei, X. Yang, J. Huang, F. Zhang, and L. Liu, "Identification of model-free hysteretic forces of magnetorheological dampers embedded in buildings under unknown excitations using incomplete structural responses," *Structural Control and Health Monitoring*, vol. 28, no. 5, p. 2715, 2021.

[44] J. He, X. Zhang, M. Qi, and B. Xu, "Model-free identification of nonlinear restoring force with modified observation equation," *Applied Sciences*, vol. 9, no. 2, p. 306, 2019.

[45] H. Su, X. Yang, L. Liu, and Y. Lei, "Identifying nonlinear characteristics of model-free MR dampers in structures with partial response data," *Measurement*, vol. 130, pp. 362–371, 2018.

[46] B. Zheng, P. Fu, B. Li, and X. Yuan, "A robust adaptive unscented Kalman filter for nonlinear estimation with uncertain noise covariance," *Sensors*, vol. 18, no. 3, p. 808, 2018.

[47] R. Mehra, "Approaches to adaptive filtering," *IEEE Transactions on Automatic Control*, vol. 17, no. 5, pp. 693–698, 1972.

[48] J. N. Yang, S. Lin, H. Huang, and L. Zhou, "An adaptive extended Kalman filter for structural damage identification," *Structural Control and Health Monitoring*, vol. 13, no. 4, pp. 849–867, 2006.

[49] J. N. Yang, S. Pan, and H. Huang, "An adaptive extended Kalman filter for structural damage identifications II: unknown inputs," *Structural Control and Health Monitoring*, vol. 14, no. 3, pp. 497–521, 2007.

[50] K. V. Yuen and S. C. Kuok, "Online updating and uncertainty quantification using nonstationary output-only measurement," *Mechanical Systems and Signal Processing*, vol. 66-67, pp. 62–77, 2016.

[51] R. Astroza, A. Alessandri, and J. P. Conte, "A dual adaptive filtering approach for nonlinear finite element model updating accounting for modeling uncertainty," *Mechanical Systems and Signal Processing*, vol. 115, pp. 782–800, 2019.

[52] A. Almagbile, J. Wang, and W. Ding, "Evaluating the performances of adaptive Kalman filter methods in GPS/INS integration," *Journal of Global Positioning Systems*, vol. 9, no. 1, pp. 33–40, 2010.

[53] Z. N. Akhlaghi and Z. Huang, "Adaptive adjustment of noise covariance in Kalman filter for dynamic state estimation," in *Proceedings of the IEEE Power & Energy Society General Meeting*, pp. 1–5, IEEE, Chicago, IL, USA, July 2017.

[54] Q. Zhang, Y. Yang, Q. Xiang, Q. He, Z. Zhou, and Y. Yao, "Noise adaptive Kalman filter for joint polarization tracking and channel equalization using cascaded covariance matching," *IEEE Photonics Journal*, vol. 10, pp. 1–11, 2018.

[55] H. Zhou and P. M. Frank, "Strong tracking filtering of nonlinear time-varying stochastic systems with coloured noise: application to parameter estimation and empirical robustness analysis," *International Journal of Control*, vol. 65, no. 2, pp. 295–307, 1996.

[56] H. Zhang, J. Xie, J. Ge, W. Lu, and B. Zong, "Adaptive strong tracking square-root cubature Kalman filter for maneuvering aircraft tracking," *IEEE Access*, vol. 6, pp. 10052–10061, 2018.

[57] D. J. Jwo and S. H. Wang, "Adaptive fuzzy strong tracking extended Kalman filtering for GPS navigation," *IEEE Sensors Journal*, vol. 7, no. 5, pp. 778–789, 2007.

[58] Y. Du, H. Zhang, L. Zhao, and W. Li, "Time-varying parametric identification of nonlinear structural systems based on STUKF," *Journal of Vibration and Shock*, vol. 36, 2017.

[59] C. C. Ji, P. C. Tuan, and H. Y. Jang, "A recursive least-squares algorithm for on-line 1-D inverse heat conduction estimation," *International Journal of Heat and Mass Transfer*, vol. 40, no. 9, pp. 2081–2096, 1997.

[60] P. C. Tuan, S. C. Lee, and W. T. Hou, "An efficient on-line thermal input estimation method using Kalman filter and recursive least square algorithm," *Inverse Problems in Engineering*, vol. 5, no. 4, pp. 309–333, 1997.

[61] L. Lennart, *System Identification: Theory for the User*, PTR Prentice Hall, Upper Saddle River, NJ, USA, 1999.

[62] C. Paleologu, J. Benesty, and S. Ciochina, "A robust variable forgetting factor recursive least-squares algorithm for system

identification," *IEEE Signal Processing Letters*, vol. 15, pp. 597–600, 2008.

[63] S. W. Pan, H. Y. Su, H. Wang, and J. Chu, "The study of joint input and state estimation with Kalman filtering," *Transactions of the Institute of Measurement and Control*, vol. 33, no. 8, pp. 901–918, 2010.

[64] F. Casciati, S. Casciati, and M. Vece, "Validation range for KF data fusion devices," *Acta Mechanica*, vol. 229, no. 2, pp. 707–717, 2018.

[65] A. B. Ricardo and L. Oliveira, "Combining strain and acceleration measurements for random force estimation via Kalman filtering on a cantilevered structure," *Journal of Sound and Vibration*, vol. 469, pp. 1–14, 2019.

[66] D. Simon, *Optimal State Estimation: Kalman, H Infinity, and Nonlinear Approaches*, John Wiley & Sons, Inc, Hoboken, NJ, USA, 2006.

[67] H. Ebrahimian, R. Astroza, and J. P. Conte, "Extended Kalman filter for material parameter estimation in nonlinear structural finite element models using direct differentiation method," *Earthquake Engineering & Structural Dynamics*, vol. 44, no. 10, pp. 1495–1522, 2015.

[68] H. Wang, Z. Deng, B. Feng, H. Ma, and Y. Xia, "An adaptive Kalman filter estimating process noise covariance," *Neurocomputing*, vol. 223, pp. 12–17, 2017.

[69] S. Eftekhar Azam, E. Chatzi, and C. Papadimitriou, "A dual Kalman filter approach for state estimation via output-only acceleration measurements," *Mechanical Systems and Signal Processing*, vol. 60-61, pp. 866–886, 2015.

[70] L. Wang, J. Guo, and I. Takewaki, "Real-time hysteresis identification in structures based on restoring force reconstruction and Kalman filter," *Mechanical Systems and Signal Processing*, vol. 150, Article ID 107297, 2021.

[71] M. Song, R. Astroza, H. Ebrahimian, B. Moaveni, and C. Papadimitriou, "Adaptive Kalman filters for nonlinear finite element model updating," *Mechanical Systems and Signal Processing*, vol. 143, Article ID 106837, 2020.